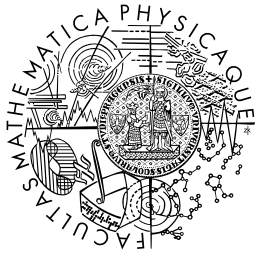

FACULTY
OF MATHEMATICS
AND PHYSICS
Charles University

BACHELOR THESIS

Kristián Vitovský

A Study of the Long-term Brightness and Colour Variations of the Be Star 88 Herculis

Astronomical Institute of Charles University

Supervisor of the bachelor thesis:	prof. RNDr. Petr Harmanec, DrSc.
Study programme:	Physics
Study branch:	General Physics

Prague 2019

I declare that I carried out this bachelor thesis independently, and only with the cited sources, literature and other professional sources.

I understand that my work relates to the rights and obligations under the Act No. 121/2000 Sb., the Copyright Act, as amended, in particular the fact that the Charles University has the right to conclude a license agreement on the use of this work as a school work pursuant to Section 60 subsection 1 of the Copyright Act.

In ..... date ..... signature of the author

I would like to express my gratitude to my supervisor prof. RNDr. Petr Harmanec, DrSc. for all the guidance, support and advice he has given me. Without his everlasting patience this thesis would be but a crumpled up piece of paper pretending it does not exist.
A great Thanks belongs to Dr. Hrvoje Božić, dipl. ing. for so graciously welcoming me at the Hvar Observatory, teaching me with the photometer and getting me through the last few late nights working on this thesis with his kind smiles and encouraging words. My thanks also go to all the people working and staying at the Hvar Observatory during my stay there for the friendly welcome and encouragement. I thank Bc. Alžběta Oplištilová for conducting observations even during her last nights on Hvar so that I could finish this.
Finally my love and gratitude belong to my mother Štěpánka Vitovská without who I would probably go mad .

Title: A Study of the Long-term Brightness and Colour Variations of the Be Star 88 Herculis

Author: Kristián Vitovský

Institute: Astronomical Institute of Charles University

Supervisor: prof. RNDr. Petr Harmanec, DrSc., Astronomical Institute of Charles Universi

Abstract: Photometric observations of the Be star 88 Herculis from 13 different sources were collected covering a period from 1968 to 2019 for the purpose of studying variations on the timescale of years to decades. All the used data was either available in or transformed into the Johnson Standard system. Since systematic photometric observations began in the 1970's the star underwent three long-term variation cycles that differ in strength and length. A quantitative description of each cycle is given. The data suggests that the star is also changing on an even longer timescale in both luminosity and colour. The photometric data was compared to the evolution of the Hα emission line and discussed in connection to possible physical models. It is shown that he object exhibits behavior that corresponds to what is described as the Negative correlation.

Keywords: 88 Herculis Be-stars Photometric variable Emission-line

Contents

Introduction

The so called Be phenomenon has been studied for more than a 150 years and yet it remains an unsolved mystery of stellar astrophysics. Be stars exhibit spectral and photometric variations on all yet observed timescales. This together with their rapid rotational velocities makes then attractive puzzle to solve as they could pose as interesting astrophysical laboratories and further the understanding of the effects of rotation on stellar objects. Many models trying to provide a general physical explanation of their behavior have been suggested but till this day all face problems and yet the last few decades have brought progress. The widely accepted assumption is that Be stars have large gaseous Keplerian disks that vary in size in time. Simultaneous numerical modeling (motivated also by other fields of astrophysics such as the study of protoplanetary disks) and systematic observations have allowed more detailed models to be considered. This thesis tries to contribute to the effort by describing variations in light and colour of one Be binary on the timescale of years to decades.

The Be star 88 Herculis was the first spectroscopic binary discovered by the 2 meter telescope at Ondřejov observatory. Systematic photometric observations began in the early 1970's and continue till this day. A majority of the observations used in this thesis were conducted at the Hvar observatory in Croatia. Observations presented covered an interval from 1968 to July 2019, to our knowledge earlier observations do not exist. Since systematic observations began 88 Her underwent three cycles of long term variations. Their description and interpretation is the aim of this thesis.

We will motivate the study of 88 Her with a brief overview of the knowledge of the nature of Be stars.

1. A Brief Overview of the Study of Be Stars

1.1 Descriptive definition

The problem of formulating a general definition of Be stars is a reflection of the current state of knowledge of their nature. In the absence of a fully adopted physical explanation; the formulation must be completely dependent on their observational properties. As we will later discuss; it has been accepted that Be stars have extensive gaseous disks. There are a few different models explaining the origin of these disks and it is unclear which one is realized. It may be that different mechanisms are in effect for different objects.
Still today the most widely quoted definition is one that was in its final form suggested by Collins [1987]

Definition 1 (Classical Be Stars)**.** *A non-supergiant B star whose spectrum has, or had at some time, one or more Balmer lines in emission*

It is clear that the physical context of all stars meeting the requirements of this definition will be an unhomogeneous group. All stars with a B V - B III spectrum for which a Balmer emission has been observed are encompassed. It is to be further noted that all B-type stars with circumstellar gas with a density at or over $10^{-13}\mathrm{gcm}^{-3}$ will show Balmer line emission, regardless the origin of the matter or the way it is kept in the environment (Rivinius et al. [2013]).
To exclude objects of similar observational properties but with identified different physical origins the term Classical Be Stars is often used. They can be otherwise defined as stars that strictly satisfy the observational conditions of the definition of Be stars excluding taxonomically similar objects like Herbig Stars, Mass Transferring Binaries, B[e] Stars and Stars with Emission Line Magnetospheres. That is excluding objects with a proven different physical source of emission than a decretion disk as is described on the basis of the model described later in 1.3.1 (Rivinius et al. [2013]).

It can be argued that with the current state of knowledge it is too soon to start excluding any objects at all for without a complete understanding it cannot be disproven that some of the objects may represent important chapters of the whole evolutionary tale. For this reason let us state a definition used in early research of Be stars (Harmanec [1983]).

Definition 2 (A very broad definition of Be stars)**.** *A B-type star whose spectrum has, or had at some time exhibited HI Balmer line emission.*

1.2 The Variations in Time of Be Stars as Observed

The most prominent aspect of the observed nature of Be stars is their dramatic variability on basically all yet studied timescales. Even though the effects often

are not very strong they constitute a unique phenomenon often termed in literature as the "Be phenomenon". Since the variability of a Be star in longer time intervals is the theme of this thesis, let us motivate further inspection of Be stars in general by describing the different types of variability observed. It is advantageous to divide the description into three characteristic timescales (Harmanec [1983]):

in 1.2.1 Short-term variations will be discussed. With characteristic time intervals of $0^{d}.1$ to several days.

in 1.2.2 Medium-term variations will be discussed. With characteristic time intervals of days to months.

in 1.2.3 Long-term variations will be discussed. With characteristic time intervals of years to decades.

1.2.1 Short-term Variations

The study of these rapid variations face many observational difficulties and a lot remains in such a state where interpretations of the obtained data can be dangerous and misleading. For Be stars changes on this time-scale have small amplitudes (smaller than $0^{m}.1$) and have not been proven for many objects. The characteristic time intervals around one day implies a further complication for obtaining good data; it is impossible to observe all parts of the change with a single instrument. Determining a possible period can be complicated by aliases created by the specific spacing of the observations (Harmanec [1983]).

Short-term variations are usually periodic with periods close to the rotational periods of the specific Be stars. For periodic short-term variations light-curves can be generally very complicated but two types can be mentioned for this basic investigation (Harmanec [1983] , Rivinius et al. [2013], Harmanec, Brož [2011]):

1. An approximately sinusoidal curve with a period P. This type of evolution is usually explained by non-radial pulsations of the object.

2. A curve alternating between local maxima and minima with a period of $2P$. In the course of a period two slightly different minima and two approximately same maxima are reached. This is interpreted as the light-curve of eclipsing contact binaries or as an effect caused by rotation and co-rotating structures in the gas above the photosphere.

Other types can be changes in the contour of the spectrum. These spectral variations also seem to be periodic or even multi-periodic.

- Changing asymmetry of spectral lines.

- Waves in the contour moving from the UV part of the spectrum towards the red part of the spectrum similar as are known to be caused by sectoral non-radial pulsations for rotating stars.

A distinct feature of short-term variations is the fact that they are observed even in times when hydrogen emission lines are not visible, which could be a clue to their origin.

1.2.2 Medium-term Variations

Variations taking place on the scale of days can often be attributed to binarity. For many systems a secondary component has been found and the observed changes seem to be phase dependent. Sensible models can be formulated taking binarity into account. Few examples of observed medium-term variations will be listed. Many of the variations on this time scale are often similar to the long-term variations described in 1.2.3 but with shorter cycle lengths and smaller amplitudes (Harmanec [1983] , Harmanec, Brož [2011]).

- Periodic RV variations, which can often (but not always) indicate binarity.
- Short intervals of visible shell lines. A geometric explanation connected to binarity has been suggested: the shell is gas originating from mass transfer between the components projected onto the Be star. The variations can be attributed to changing rate of matter ejection in the equatorial region and revolution of the whole binary system.
- Hα V/R variations (see 1.2.3) on this time-scale. If phase-locked a natural interpretation seems to be the presence of a rotating asymmetric disk in a revolving binary system. Then for example for a disk rotating against the sense of the revolution of the binary system we should observe V>R when RV is positive and vice versa.
- Periodic variations in light, colour and line profiles can be observed for Be binaries.
- A great number of variability corresponding to this time-scale has been observed in the far UV region, notably distinct variability has been documented for resonance lines especially C IV. For these resonance lines narrow second lines shifted towards the blue region of the spectrum are observed as substantially changing.

1.2.3 Long-term Variations

Long-term variations are the most observationaly distinct effects. Let us point out the known variations:

E/C Variations

The strength of Balmer emission lines relative to the spectral continuum changes in cycles of about 10 to 30 years. Cycles are known in different shapes and sizes. If we denote a B-type spectrum with a double peaked H α emission line and an absorption core as if further described in 1.3.1 of a *Be shell* spectral type and a B-type spectrum with a simple H α emission line as of a *Be* spectral type, the typical cycles would be (Harmanec [1983]):

$$\begin{gathered} B \rightarrow Be \rightarrow Be \;\; shell \rightarrow Be \rightarrow B \\ Be \rightarrow Be \;\; shell \rightarrow Be \\ B \rightarrow Be \rightarrow B \end{gathered}$$

V/R Violet to Red and RV Radial Velocity Variations

Cyclic changes of the ratio of peak intensities of the double-peaked emission lines. Let us summarize the observed tendencies of these variations (Okazaki [1991]Harmanec [1983] , Rivinius et al. [2013], Harmanec, Brož [2011]) :

- V/R variations are cyclic but not strictly periodic. The amplitude of the effect and cycle lengths may vary from cycle to cycle.
- Cycles have characteristic lengths from years to decades with a statistical mean at 7 years. The variations usually disappear after several cycles and reappear again in 10-30 years. Cycle lengths are not dependent on the spectral subclass.
- The phenomenon is connected to simultaneous changes in radial velocities of both peaks and the absorption core.
- The whole contour shifts towards the red part of the spectrum when V>R and vice versa.
- For certain binary shell systems these V/R variations have been observed to be in phase with orbital motion (as discussed in 1.2.2).
- For certain shell stars a third peak or a non-central absorption core has been observed in a short time interval when V $\approx$ R in a variation going from V<R to V>R. Cases where even a fourth non-central absorption core have been documented this is likely due to self-absorption in a very massive disk of the Be star.

Correlation between Photometric and Spectral Variability

Be stars are long-term photometric variables. Studies of correlation between spectral and photometric variability have shown two prominent types of correlation (Harmanec [1983] , Rivinius et al. [2013], Harmanec, Brož [2011]):

- **Positive correlation**

  Definition 3 (Positive correlation)**.** *For a certain system there is a positive correlation between the strength of Balmer emission and luminosity. That is the stronger the emission the brighter the star.*

  This type of correlation has been found for example for π Aqr, μ Cen or γ Cas.
  For stars exhibiting this kind of correlation some other typical observables have been recognized:

  - During the initial increase in luminosity i V the $B-V$ gets redder and the $U-B$ gets bluer.
  - The body moves in the $U-B$ vs $B-V$ diagram from the luminosity class V. to Ia without a spectral type change.
  - During the brightening the $V-R$ increases by more than $0^{\mathrm{m}}.1$.

- **Negative correlation**

  Definition 4 (Negative correlation)**.** *For a certain system there is an inverse correlation between the strength of Balmer emission and luminosity. That is the stronger the emission the fainter the star.*

  This type of correlation has been documented for example for 88 Her, 28 Tau and V1294 Aql.
  Again let us list typical behavior connected to stars exhibiting this correlation.

  - During the decrease in luminosity in V both $B-V$and $U-B$ indices redden.
  - The body moves in the $U-B$ vs $B-V$ diagram along the main sequence but does not change it's luminosity class.
  - During the shell formation phase the stars have wide Ca II K lines in their spectra.

1.3 Possible models of disk origins

It is now generally accepted that the presence of Balmer emission in Classical Be stars originates in large gaseous Keplerian disks around the central star. The circumstelar material has its origins in the central object but the mechanism of ejection remains unexplained. Many physical explanations have been suggested but even today all face problems. Let us now summarize the most important ideas.

1.3.1 Critical rotation

Struve [1931] showed a correlation between the width of emission lines in Be star spectra and the observed speed of rotation $v \cdot \sin i$ where v is the tangential speed of rotation on the equator and i is the inclination of the star. The model Struve suggested can be summarized in the following way:

- Be stars are objects rotating at critical speed, that is when centrifugal forces cancel out gravity:
  $$\frac{GM_*}{R^2} = \frac{v_c^2}{R} \tag{1.1}$$
  The critical speed of rotation is given by:
  $$v_c = \sqrt{\frac{GM_*}{R}} \tag{1.2}$$
  Where the G is the gravitational constant, M_* the mass of the star and R the equatorial radius of the star. Fast rotation deforms the star into a lens-like shape. At critical rotation due to a pressure gradient matter can stream from the equatorial region creating a decretion disk. If we take into consideration the aforementioned deformation of the star and that the equipotential surfaces are also sufaces of constant density, we can assume

that the star will take the shape of a Roche model. We can derive (Harmanec, Brož [2011])

$$v_c = \sqrt{\frac{2}{3}\frac{GM_*}{R_{pole}}} = \sqrt{\frac{GM_*}{R_{equator}}} \tag{1.3}$$

- This model also brings a geometric interpretation of the different shapes of emission lines and allows an theoretical prediction of the contours (Struve [1931]).
  - If the inclination i of the axis of rotation is close to 90° we observe an emission line that is double peaked, this is caused by the fact that the observer sees cirmustellar matter flowing towards and away from him as it rotates around the central star (Harmanec, Brož [2011]) . If we take the classical Doppler effect:

    $$\lambda = \lambda_0 \left(1 + \frac{RV}{c}\right) \tag{1.4}$$

    we can see that there is a dependence between the radial velocity RV and the wavelength λ. Where λ_0 is the wavelength at $RV = 0$ and c denotes the speed of light. To obtain a theoretical contour of an emission line let us consider a ring instead of a disk around the central star. We assume that the ring is thin enough that there is no difference in the speed of rotation v between its inner and outer circumference. We can calculate RV for each point:

    $$RV = v \sin i \sin \alpha \tag{1.5}$$

    where α is the angle at the center of the star defined by the line of sight and the direction to the point. If we invert the equation so that we get an expression for α and choose sufficiently small steps in RV so that for the interval (α_{n-1}, α_n) we can assume the same value of radial velocity:

    $$RV_{interval} = \frac{RV_n - RV_{n-1}}{2} \tag{1.6}$$

    then the intensity for each step will be proportional to the difference in α: $I = const \cdot (\alpha_n - \alpha_{n-1})$. From 1.5 we get:

    $$(\alpha_n - \alpha_{n-1}) = \arcsin\left(\frac{RV_n}{v \cdot \sin i}\right) - \arcsin\left(\frac{RV_{n-1}}{v \cdot \sin i}\right) \tag{1.7}$$

    Equation 1.7 gives a theoretical prediction of the shape of a single emission line. In this calculation we neglected that RV depends on the distance from the star, this will make a real line smoother. Also other effects were not taken into consideration such as absorption in the disk, the transfer of radiation, the size of the star or the thickness of the disk.
  - If i of the axis of rotation is close to 0°the rotation of the disk will not affect the contour and we will observe a narrow single peaked emission line.

This geometric explanation also brings under the term Be stars the so called Shell stars, where shell stars are objects observed through the edge of the disk(Rivinius et al. [2013].).

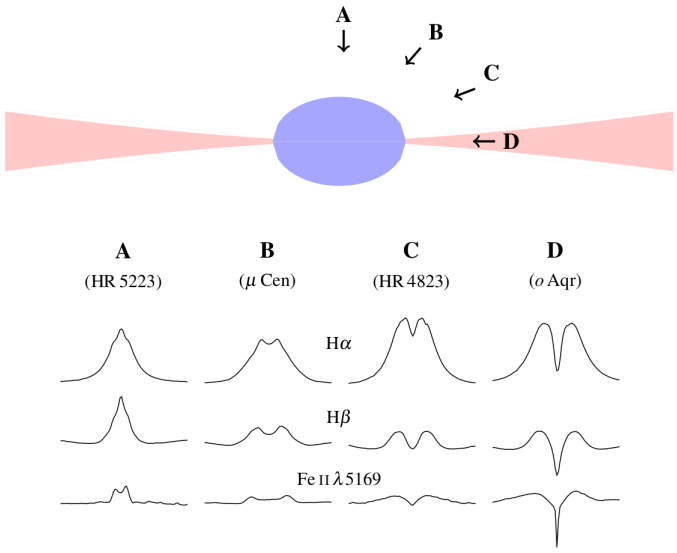

Figure 1.1: An overview of Be star spectra in Struve's model of critical rotation as seen under different inclinations. Taken from Rivinius et al. [2013].

Observations show that most Be stars have a high value of $v \cdot \sin i$ and so are fast rotating and statistically we can conclude that all Be stars rotate rapidly (that is objects with low values of $v \cdot \sin i$ are observed pole-on) (Harmanec, Brož [2011]). Despite this, further measurements seem show that Be stars reach only 70%-80% of critical speeds. Let us note that all estimates of what fraction of critical rotational velocity Be stars really reach remain dependent on the assumed masses of the stars, which have not been directly measured. Masses of Be stars are determined statistically based on the observed spectral type which can be influenced by the so called pseudophotosphere (photosphere mimicked by the disk). What we can still assume today is that rapid rotation, although not itself the cause of matter ejection, can weaken the effective gravity and so weaker effects can come into play.
The model also fails to explain the dramatic variations in time that all Be stars typically exhibit, although the geometric explanation can provide an idea of the cause of the two prominent correlations between emission and luminosity (Harmanec [1983]).

Positive correlation; If an object is viewed roughly pole-on the growth of the disk (observed as the increase in emission) can simulate the growth of the star (observed as the increase in luminosity). The star will move towards the supergiants in the $U-B$ vs $B-V$ diagram. Considering a very flat disk, this could also explain why this type of correlation is more frequent.

Negative correlation; If an object is viewed through the disk (that is with i close to 90°) then the envelope will cause a greater shielding of the central star

resulting in a decrease in luminosity. The cooler disk can simulate the photosphere of a later spectral type hence explaining the travel in the $U-B$ vs $B-V$ diagram along the main sequence.

1.3.2 Mass-transferring binary models

In the definition of Classical Be stars mass-transferring binaries have been excluded, since the source of emission lines is different than a decretion disk. Kříž and Harmanec [1975] suggested that some Be star observables can be explained if we consider a close binary system with a secondary that fills the Roche lobe. The gaseous disk around the more massive primary of an early spectral type is an accretion disk formed from a case B mass transfer. The model brings a good explanation of the high rotational velocities of Be stars as a consequence of extra angular momentum from the matter falling onto the star, double peaked emission lines and their different shapes here caused by the asymmetry of the disk and the streaming matter. Some long-term variations in time could also be explained.
Observations speak against the aforementioned model as a general explanation; if all Be stars were to have companions filling he Roche lobe there would statistically have to be a much greater number of Be eclipsing binaries observed, also for certain Be binary objects the possibility of such a secondary has been disproven since they are small hot stars. Harmanec et al. [2002] formulated a second model. Let us first discuss the Roche model (Harmanec,P, Mayer,P, Zache P [2019]).

Roche model

We will describe a binary system as a constrained three-body problem. Let us assume two bodies with their masses M_1, M_2 concentrated in their centers of mass locked together only by gravitational interaction, we will set the distance between them to $a = 1$, the two bodies move in circular orbits around the CM (center of mass) of the system in synchronous rotation (that is the angular velocities of rotation of both stars equal to the angular velocity of the rotational revolution of the system). Let us choose a co-rotating Cartesian coordinate system with an origin in M_1 with the z-axis parallel to the vector of angular momentum of the system and the x-axis in the direction of M_2. If we place a test particle m ($m << M_1,\ m << M_2$) in $\vec{r}_1 = (x, y, z)$ there are three forces acting on it: Newtonian gravitational pull from both bodies and the centrifugal force.

$$\vec{F}_{final} = -G\frac{mM_1}{r_1^3}\vec{r}_1 - G\frac{mM_2}{r_2}\vec{r}_2 + m\omega^2\vec{r}_3 \tag{1.8}$$

where G is the gravitational constant, $\omega = \frac{2\pi}{P}$ is the angular frequency of the binary system(P is it's period), $\vec{r}_2 = (1-x, y, z)$ defines the position of m relative to M_2 and $\vec{r}_3 = (x - \frac{M_2}{M_1+M_2}, y, z)$ defines the position of the projection of m onto the plane of rotation ($z = 0$). The potential W in $\vec{r}_1$ is given by (with a reference point chosen so that it is negative):

$$W(x, y, z) = -\frac{GM_1}{r_1} - \frac{GM_2}{r_2} - \frac{1}{2}\omega r_3^2 \tag{1.9}$$

Using the third Kepler law to express ω (the distance between M_1 and M_2 is $a = 1$):

$$\omega^2 = G(M_1 + M_2) \tag{1.10}$$

and rewriting 1.9 with the mass fraction $q = \frac{M_2}{M_1}$ yields:

$$\frac{W(\vec{r}_1)}{GM_1} = -\frac{1}{(x^2+y^2+z^2)^{\frac{1}{2}}} - \frac{q}{((1-x)^2+y^2+z^2)^{\frac{1}{2}}} - \frac{1+q}{2}(x^2+y^2) + qx - \frac{q^2}{2(q+1)} \tag{1.11}$$

We can now point out two observations:

1. The shape of the equipotential planes depends solely on the value of q.
2. The last term in 1.11 does not effect the shape of the equipotential planes just the value of the potential.

We can define a new so called Kopal potential (Kopal [1959]):

$$K(\vec{r}_1) = \frac{W(\vec{r}_1)}{GM_1} + \frac{q^2}{2(q+1)} \tag{1.12}$$

The equipotential surfaces are yielded as solutions of:

$$K = const \tag{1.13}$$

At equilibrium a star will take the shape of an equipotential plane. Important for dynamical stability are points of force equilibrium, which are yielded as solutions of $\nabla K = 0$:

$$\frac{\partial K}{\partial x} = \frac{\partial K}{\partial y} = \frac{\partial K}{\partial z} = 0 \tag{1.14}$$

The so called Lagrangian points are denoted L_i in 1.3.2. L_1 is located in the same place as the already mentioned Roche-lobe that represents the limit of the dynamical stability of a star, that is if one star fills the Roche-lobe mass transfer will occur in the vicinity (semi-detached binaries) and if the binary system fills a greater plane (greater than plane 3 in 1.3.2) the two stars will share an atmosphere (contact binaries). This simple Roche model omits the Coriolis force and the pressure gradient, so in reality the balance in L_1 is disturbed and matter will stream towards the companion as soon as the Roche-lobe is filled. The position of L_1 can be calculated if we notice that $\frac{\partial K}{\partial y}$ and $\frac{\partial K}{\partial z}$ are zero on the x-axis:

$$\frac{\partial K(x,0,0)}{\partial x} = \frac{x}{\mid x \mid^3} - \frac{q(1-x)}{\mid (1-x) \mid^3} - (1+q)x + q = 0 \tag{1.15}$$

for L_1 we can restrict x to (0,1) and so get rid of the absolute value. This can be rewritten as:

$$x_{L_1}^{-2} - x_{L_1} = q((1-x_{L_1})^{-2} - (1-x_{L_1})) \tag{1.16}$$

Harmanec et al. [2002] model

The simple Roche model assumes three main simplifications:

1. $M_1,\ M_2$ are mass points.
2. Synchronous rotation.

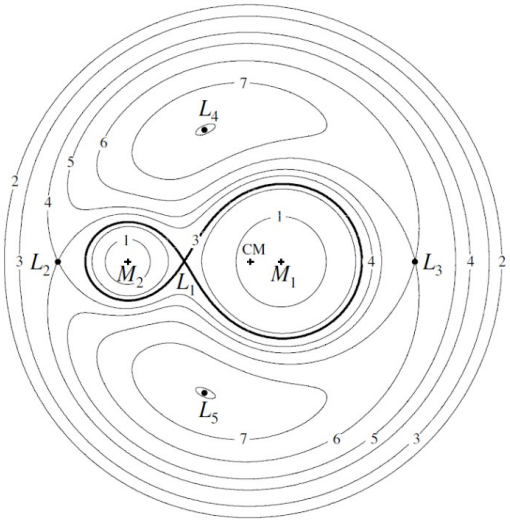

Figure 1.2: Roche model equipotential planes and Lagrangian points (Skelton and Smits [2009]).

3. Axes of rotation of the two bodies are perpendicular to plane of rotation of the binary system.

Harmanec et al. [2002] extended the effort by considering a model under more general assumptions. They assumed rapid asynchronous rotation where the angular velocity of the primary is not equal to the angular velocity of the revolution of the binary system $\omega_* \neq \omega$ but the vectors of angular momentum are still parallel. Under these assumptions in the co-rotating coordinate system we will have to add terms for the centripetal a Coriolis force into the potential 1.9:

$$W_A(x, y, z) = W(x, y, z) - \frac{1}{2}(\omega_*^2 - \omega)(x^2 + y^2) \tag{1.17}$$

Let us study the position of the limiting point for dynamical stability L_{1A} (that is when matter can be ejected towards the companion) under the aforementioned assumptions. Once again the Lagrangian points are yielded by $\nabla W = 0$, which for L_{1A} gives:

$$x_{L_{1A}}^{-2} - B^2 x_{L_{1A}} = q((1 - x_{L_{1A}})^{-2} - (1 - B^2 x_{L_{1A}})) \tag{1.18}$$

where $B = \frac{\omega_*}{\omega}$. Let us discuss what 1.18 implies as pointed out by Harmanec et al. [2002]:

- The sign of B does not effect the solution.
- The size of the Roche lobe is affected by the value of B:
  - for $B < 1$ we get $x_{L_{1A}} > x_{L_1}$ and the Roche lobe is larger than in the simple Roche model.

  - for $B > 1$ we $x_{L_{1A}} < x_{L_1}$ and the Roche lobe is smaller than in the simple Roche model. As B approaches infinity $x_{L_{1A}}$ approaches zero.

- For a single star a particle needs parabolic energy to escape the system but in a binary system a particle needs only a high enough energy to reach L_1, where it can be attracted by the gravity of the companion.

- We observe that for a rapidly rotating star the energy for matter ejection is lower than in the simple Roche model. If we compare the potential from 1.9 in L_1 with the sum of this potential in L_{1A} and the kinetic energy a particle gains from stellar rotation:

$$W(L_{1A}) + \frac{1}{2}(\omega_* - \omega)x_{L_{1A}})^2 < W(L_1) \tag{1.19}$$

  we can conclude that mass transfer to the companion will not occur.

- Particles that do not reach L_1 move in closed trajectories around the star forming a gaseous Keplerian disk.

Let us underline the important amendment that binary models bring to mass ejection and the formation of the disk; mass ejection does not occur in the whole equatorial region but only in the direction of the first Lagrangian point. The key struggle of the model lies in the fact (as shown by further simulations) that for the disk to be created rotational velocities of around 98% are still required. At such rotational velocities other effects are to be also considered.

1.3.3 Non-radial pulsation model

This model emerged from observations of the multi-periodic Be star μ Cen and was suggested as a general explanation (Baade [1988], Rivinius et al. [2013]). As we have discussed earlier Be stars exhibit rapid rotation but generally do not reach critical rotation. The fast rotational velocities lower the effective gravity and so the kinetic energy of matter that needs to be added for critical kinetic energy to be reached and ejection in the equatorial region to be possible can be attributed to weaker effects. High rotational velocities of Be stars implicate multi-periodicity.
Let use first formulate a mathematical description of pulsation velocity fields for different modes (Harmanec, Brož [2011]). Each mode is defined by quantum numbers $l,\ m,\ n$ denoting

n is the number of pulsation waves in the radial direction,

l is the number of nodes on the stellar surface,

m is the number of pulsation waves in the azimutal direction.

If we choose a set of spherical coordinates $(r,\ \theta,\ \phi)$ and using spherical harmonics $Y_l^m(\theta, \phi)$ the elements of the velocity field vectors are yielded by:

$$V_r(r, \theta, \phi) = A_n(r)Y_l^m(\theta, \phi)e^{i\omega_{nlm}t} \tag{1.20}$$

$$V_\theta(r,\theta,\phi) = A_n(r)k\frac{\partial Y_l^m(\theta,\phi)}{\partial\theta}e^{i\omega_{nlm}t} \tag{1.21}$$

$$V_\phi(r,\theta,\phi) = \frac{A_n(r)}{\sin\theta}k\frac{\partial Y_l^m(\theta,\phi)}{\partial\phi}e^{i\omega_{nlm}t} \tag{1.22}$$

where $A_n(r)$ denotes the corresponding amplitude, $\omega_{nlm}t$ yields the corresponding phase in time t and k is the ratio of the amplitude of the horizontal velocity and of the radial velocity.
Simple non-radial pulsation can not explain matter ejection because the velocity fields created by it are globally limited by the speed of sound in the stellar enviroment, greater local velocity gradients will not survive long. The amplitudes of such pulsation velocity fields reach only about $\approx$ 20km s^{-1} (Rivinius et al. [2013]).
This limit can be overcome at moments of constructive interference of different modes of pulsation, then the amplitudes of the population velocity fields can for some time reach values much higher then the speed of sound limit. The pulsation velocity fields of the the modes add up on the whole surface of the star. In the equatorial region this effect can compensate for the excess kinetic energy needed for matter ejection to occur ((Rivinius et al. [2013]).
For μ Cen matter ejection is observed for constructive interference of modes for which:

$$l_i = l_j; \quad m_i = m_j; \quad n_i \neq n_j; \tag{1.23}$$

Interference of modes of different l and m will be much less effective for mass ejection because as we see in the equations describing the corresponding velocity fields hidden inside the spherical harmonics the distribution on the stellar surface will be different (Rivinius et al. [2013]).
Spectroscopic observations speak against this model in the sense that the constructive interference of the desired modes seems to be uncommon. Another problem can emerge if we consider retrograde pulsation waves ($m > 0$, that is against the sense of stellar rotation) because they will transport angular momentum from the uppermost layers of the stellar atmosphere if damped there so working against matter ejection (Rivinius et al. [2013]).

2. Of Photometry at Hvar Observatory

This bachelor thesis is motivated by almost 50 years of systematic observations at Hvar Observatory in Croatia. The observatory was founded in 1972 as a joint venture of Czechoslovakian and Yugoslavian scientists (Harmanec and Božić [2013]). A great fraction of data used for the analysis of long-term variations of 88 Her used here were obtained at Hvar. This chapter will briefly look upon the specifics of photometric observations conducted at Hvar.

2.1 The Johnson UBV System

The Johnson UBV system is the most widely used photometric system. It is defined by measurements of a large number of constant stars in three filters (Harmanec,P [2019]). The magnitude of a star outside of the Earths atmosphere is

Table 2.1: Johnson UBV system definition (Johnson and Morgan [1953])

Filter	Lower wavelength limit [nm]	Maximum effectivity [nm]	Upper wavelength limit [nm]
U	300	360	420
B	360	420	560
V	460	535	740

determined by comparison of instrumental magnitudes of the observed star and the well-known constant Johnson Standard stars, that is measurements are carried out differentialy.
At Hvar Observatory an fourth filter is now used; R with a maximum effectivity at 700 nm extending the measurements into the red part of the spectrum (Harmanec,P [2019]).

2.2 The Method of Reduction Used at Hvar Observatory

The value of data obtained at Hvar lies in the strategy chosen for their reduction. Photometric measurements at Hvar face uneasy conditions, this motivated the observers to approach the reduction of all measurements with extreme care. Two main ingredients are to be mentioned; 1. careful inspection is carried out for all data quickly during observations and then systematically during analysis, 2. the Fortran77 program HEC22 is used with implemented non-linear equations for modeling extinction and colour perturbation by the instrument. Let us summarize calculations executed by HEC22.

2.2.1 Obtaining Data and Data Reduction Using Non-linear Equations

Let us summarize what is considered to obtain the *UBVR* magnitudes of variable stars in the program HEC22 (Harmanec [2017], Harmanec,P [2019]).

- Observations are carried out deferentially with respect to constant comparison stars.

- Measurements of each star in the four filters is carried out immediately one after another, to allow a better transformation (as will be discussed in a later point). The integration time for each filter is chosen with consideration of the different signals of different filters and the colours of the different stars.

- For each measurement of a studied variable star two other stars are measured successively. The *comparison* and *check* stars are chosen so that they are of a similar spectral type and as close as possible on the sky to the variable star. A third *transformation* star is chosen of a distinctively different colour and measured at the beginning and the end of an observational cycle . A whole cycle of measurements would follow the scheme:

$$\begin{gathered} \textit{Comparison} \rightarrow \textit{Check} \rightarrow \textit{Transformation} \rightarrow N \times \{\ \textit{Variable} \rightarrow \\ \textit{Comparison} \rightarrow \textit{Check}\ \} \rightarrow \textit{Control} \rightarrow \textit{Variable} \rightarrow \textit{Opposite} \rightarrow \textit{Check} \rightarrow \\ \textit{Comparison} \end{gathered}$$

  This is necessary for the observers to be able to differentiate between short-term changes in the atmosphere and real variations of the studied variable star. The role of the *check* star is a quality and constancy check.It can be used as a comparison star in case the chosen *comparison* turns out to be a variable.

- Let us consider that for the magnitude m and photon count N we get from the Pogson equation:

$$m = -2,5 \log_{10} N + O_{point} \tag{2.1}$$

  the O_{point} - zero point (reference point) is (in an idealized interpretation) a constant chosen for the instrument. This equation can be derived under the assumption that there is a linear relation between the flux Φ and the photon count N: $N(\Phi) = const\Phi$, generally this is not true. Especially for bright objects the detector can be overloaded and effectively the detector stops counting for some time interval. We can calculate a correction iteratively from:

$$N = ne^{d \cdot N} \tag{2.2}$$

  where N again represents real photon count, n the measured photon count and d is the so called 'dead-time' coefficient. Also photomultipliers can exhibit non-linearities for bright bodies. For Voltage U in volts and a constant characteristic for the specific component the correction is yielded by:

$$N = n\left(1 - \frac{n}{U \cdot const}\right) \tag{2.3}$$

- The transformation from the measured magnitudes ($v,\ b,\ u,\ r$) into the UBVR system magnitudes ($V,\ B,\ U,\ R$) considers the detected light to be influenced by two main factors: by the Earth's atmosphere and by the instrument itself. In the course of each night measurements of standard are carried out that serve the two steps of the transformation.

  – For each night or a part of night if observations were interrupted the extinction coefficients G_i are determined from the measurements of standard stars by a polynomial regression. Extinction is modeled assuming a dependence on air mass X and the time of observation t. A model is used for the calculation of X described by (Bemporad [1904]);

$$X = Q + 1 - 0,0018167Q - 0,02875Q^2 - 0,0008083Q^3 \tag{2.4}$$

  where

$$Q = \frac{1}{\cos z} - 1 \tag{2.5}$$

  It is good to obtain measurements of standards in a wide range of air masses.
  The variation of the extinction in the atmosphere during the night can be modeled in HEC22 by an polynomial of a chosen degree up to five (by fixing the appropriate G_i coefficients to zero). The degree of the polynomial used is to be chosen with care so that the fit remains determined by the physical evolution of the atmosphere and not by the uncertainty of the measurements.
  Altogether the extinction-free instrumental magnitudes ($v_0,\ b_0,\ u_0,\ r_0$) are yielded from the measured magnitudes ($v,\ b,\ u,\ r$) by:

$$\begin{pmatrix} v_0 \\ b_0 \\ u_0 \\ r_0 \end{pmatrix} = \begin{pmatrix} v \\ b \\ u \\ r \end{pmatrix} - \begin{pmatrix} G_1 & G_5 & G_9 & G_{13} & G_{17} & G_{21} & G_{25} \\ G_2 & G_6 & G_{10} & G_{14} & G_{18} & G_{22} & G_{26} \\ G_3 & G_7 & G_{11} & G_{15} & G_{19} & G_{23} & G_{27} \\ G_4 & G_8 & G_{12} & G_{16} & G_{20} & G_{24} & G_{28} \end{pmatrix} \begin{pmatrix} 1 \\ X \\ Xt \\ Xt^2 \\ Xt^3 \\ Xt^4 \\ Xt^5 \end{pmatrix} \tag{2.6}$$

  The detected light can be also perturbed (with variations of the effect on this timescale) by fluctuations of the zero point of the instrument. The program also allows the modeling of this up to a quadratic polynomial.

$$\begin{pmatrix} v_0 \\ b_0 \\ u_0 \\ r_0 \end{pmatrix} = \begin{pmatrix} v \\ b \\ u \\ r \end{pmatrix} - \begin{pmatrix} G_1 & G_5 & G_9 & G_{13} \\ G_2 & G_6 & G_9 & G_{13} \\ G_3 & G_7 & G_9 & G_{13} \\ G_4 & G_8 & G_9 & G_{13} \end{pmatrix} \begin{pmatrix} 1 \\ X \\ t \\ t^2 \end{pmatrix} \tag{2.7}$$

  – The variations in time of the influence of the instrument itself are much weaker so the colour extinction coefficients H_i can be considered constant throughout a single season (under the assumption that no technical adjustments were made to the instrument). The coefficients H_i are determined by a large number of measurements of standard

stars again by polynomial regression. The final $V,\ B,\ U,\ R$ magnitudes are yielded by:

$$\begin{pmatrix} v_0 \\ b_0 \\ u_0 \\ r_0 \end{pmatrix} - \begin{pmatrix} V \\ B \\ U \\ R \end{pmatrix} = \begin{pmatrix} H_1 & H_2 & H_3 & H_4 \\ H_7 & H_8 & H_9 & H_{10} \\ H_{13} & H_{14} & H_{15} & H_{16} \\ H_{19} & H_{20} & H_{21} & H_{22} \end{pmatrix} \begin{pmatrix} (B-V) \\ (U-B) \\ (B-V)^2 \\ (B-V)^3 \end{pmatrix}$$
$$+ X \cdot \begin{pmatrix} H_5 C_4 \\ H_{11} C_4 \\ H_{17} C_5 \\ H_{23} C_5 \end{pmatrix} \left[\begin{pmatrix} (B-V) \\ (B-V) \\ (U-B) \\ (U-B) \end{pmatrix} + \frac{1}{2} X \cdot \begin{pmatrix} C_4 \\ C_4 \\ C_5 \\ C_5 \end{pmatrix} \right] + \begin{pmatrix} H_6 \\ H_{12} \\ H_{18} \\ H_{24} \end{pmatrix}$$

where $C_i = G_{i+2} - G_{i+1}$

It has been well documented, that the use of non-linear equations for transformations brings more accurate results, than the still often used linear ones. Linear transformations frequently cause an additional error of the order $\approx 0^{\mathrm{m}}.1$.

3. A Summary of the Study of 88 Her in Time

This thesis focuses on the long-term variations in luminosity and colour of the Be binary star 88 Her, it is therefore necessary to formulate a summary of what is already known about the object. We will list the most important ideas and conclusions, it will be useful to do this in a partly chronological manner so to also underline that which has been disproven.

3.1 Notes on publications about 88 Her

1. The object was classified as a Be star by Bidelman and Svolopoulos [1960] after they observed emission and shell lines in 1959. Other authors later published earlier observations of emission lines (Herman and Duval [1962]).

2. Harmanec et al. [1972] conducted measurements of RV from spectra obtained at Ondřejov observatory and found periodical variations with a period of 80 to 90 days and an amplitude of around 10 km s^{-1} . Another shorter period close to one day was suggested as possible with the note that it probably was not true and caused by the the timing of the observations. Two models were suggested as the cause of the variations; pulsations of the extended atmosphere of the star or the star as a component of a spectroscopic binary. The authors put forth arguments on behave of the binary hypothesis and calculated orbital elements. Under the assumption that the object is of the spectral type B6 and luminosity class IV-V they estimated the mass of the primary component: 3.2 $\mathcal{M}^{\mathrm{N}}_{\odot} \leq M_1 \leq 6.6\ \mathcal{M}^{\mathrm{N}}_{\odot}$. They also calculated possible values of the mass of the secondary and the distance between the two stars. It was pointed out that the calculated values resemble computed values for a binary system 4 + 3.2 $\mathcal{M}^{\mathrm{N}}_{\odot}$undergoing the final stages of a case B mass exchange. This led them to believe that the secondary should be sought after in the red and infrared part of the spectrum. 88 Her became the first spectroscopic binary discovered in Czechoslovakia. A period of around 87 days was confirmed by Harmanec et al. [1974] from a greater number of RV measurements on spectra from Ondřejov and Haute Provence observatories, at the same time the possibility of a shorter period of around 1 day was disproven. They calculated new orbital elements. Using a test designed by Lucy and Sweeney [1971] they proved that binary had a real eccentricity and speculated that the eccentricity may connected to gas steaming between the components.

3. Harmanec et al. [1974] also discussed spectral variations.

   - Doazan [1973] (confirmed by spectra from Ondřejov) published that the metallic shell lines of the system started to disappear in 1970. By 1973 most were gone.
   - Hα emission line underwent a decrease in intensity in the period between 1971 and 1973 (Doazan [1973] , Svolopoulos [1973]).

This suggested long-term variations of the system. The fact that the intensity of Balmer lines undergoes changes but their RV curve remains the same led the authors to the conclusion that such behavior cannot be explained by the pulsation hypothesis and further calculations were conducted under the assumption that 88 Her is a binary system.

4. Then new spectroscopic evidence showed that no red-giant was present in the system (Plavec [1973] , Allen [1973]) on the other hand the spectral variations indicated the possibility of matter exchange, so the basic assumption that the system is undergoing case B mass exchange was kept, where 88 Her is the mass gaining component. This model (as was discussed in 1.3.2) could explain the observed high rotational velocities and the observed spectral variations; the varying amount of delivered angular momentum could trigger rotational instability varying in time.

5. Harmanec et al. [1974] further claimed that since wide double peaked Hα emission lines were observed (shell lines) that the object was being viewed roughly edge-on, that is through the disk as described in 1.3.1.

6. A new set of possible parameters for the secondary was computed for inclination of 50°and 90°under the assumptions: 1. the secondary fills the Roche-lobe, 2. M_1=5.4 $\mathcal{M}_{\odot}^{\mathrm{N}}$, 3. the Be primary is of spectral type B6 and luminosity class IV-V, 4. using the orbital elements computed from the new set of RV measurements (Harmanec et al. [1974]). The model and the fact that the secondary component had not been observed implied the Be star should be over-luminous in V for its spectral type or that the secondary is of spectral type late A or early F (the magnitude needed for the secondary component not to be under this assumption would not correspond to the observed spectral type B6).

7. In the 1970's systematic photometry joined the struggle at few observatories in Europe. Harmanec et al. [1978] used photometric data from five observatories covering a period from 1968 to 1977 and found **long-term variations in brightness and colour of 88 Her**. Since this is in direct connection with the theme of this thesis let us list their discoveries in more detail. The cycle numbers were calculated using the spectroscopic ephemeris available then:

$$T_{maxRV} = \mathrm{HJD2419429.251}+86^{\mathrm{d}}.7206\times E$$

- An observed change in U,B and V:

  1968-1972: steady increase in luminosity in all three filters

  1972-1976: approximately constant luminosity in all B and V (cycles 253-272).

  1977 onward: rapid decrease in luminosity in all three filters by more than $0^{\mathrm{m}}.15$ in B,V and $0^{\mathrm{m}}.3$ in U (cycles 274-277).

  The authors note that the decrease is likely caused by an event restricted to only a couple of cycles or even only one (272-274).

- In the $U-B$ versus $B-V$ diagram whilst remaining a main sequence object it changed its spectral type from B8 to B6 approximately in the first phase and from B6 to B7 in the last phase.
- In comparison to spectroscopic observations (which have been discussed earlier) the object had strong Hα emission in the decreasing (B8) phase and almost no lines were visible during the phase of constant luminosity (B6).
- They obtained an estimate of the stellar angular diameter in the different phases, which show an increase in size during the phases with shell lines.
- Under the assumption that the strength of emission is connected to the extent of the disk, they suggested the model that the disk can simulate a later spectral type and partly shields the light from the central star.

Note that the observed changes and the suggested model agree very well with what has been defined and described as a Negative Correlation in sections 1.2.3 and 1.3.1.

8. Also in the paper Harmanec et al. [1978] the possibility of variations of medium and short-term timescales were suggested, but due to insufficient data no convincing result was found.

9. Doazan et al. [1982] used spectroscopic observations covering the period 1963-1979 and *UBV* photometry covering the period 1968-1981. Periodic variations of RV were confirmed. The period around 87 days was found to have remained constant. The fact that the RV curve had not changed despite the found long-term variations was taken as a further argument on behave the binary hypothesis. New more precise orbital elements were computed. The eccentricity was confirmed as real (Lucy and Sweeney [1971]). Other variations connected to the spectroscopic period were studied:

    - An RV curve obtained from measuring the Hα emission lines deviates from the main RV curve used for orbital solutions obtained as mean values of RV for HI lines.
    - A second absorption core of Hα in the direction of the red part of the spectrum periodically appears around phase 0.25 and disappears around phase 0.30. Gradually the RV of this second absorption core decreases as its strength increases, it moves towards the ultraviolet part of the spectrum and at some point switches place with the main absorption core.
    - Phase locked V/R variations of Hα occur.
    - RV curves of other lines were measured; 1. Fe II follows the HI RV curve 2. Fe I and Ca II K do no vary with spectroscopic period.
    - No phase dependent photometric variability was found as well as no notable line-profile variations were found.

10. Long-term variations were further studied (Doazan et al. [1982]). A more precise ephemeris was used calculated with the added RV measurements.

$$T_{maxRV} = \text{HJD2419429.301} + 86^{\text{d}}.7221 \times E$$

To between cycles 242-253: Slow growth of luminosity and decrease of the strength of Balmer and metallic shell lines. The object was getting bluer. The moment when maximum luminosity in V (242-253) was reached approximately corresponds to the moment metallic when shell lines stopped being visible (250-254).

Until cycles 265-267: Hα and Ca II K shell lines continue to weaken until they disappear. In correlation colour indices get slightly redder.

Cycles 251-274: The Hβ and the Fe II(3) lines gain in intensity.

Cycles 253-272: No metallic shell lines visible and luminosity effectively constant.

Cycle 272 or 273: Observations indicate an event constrained to probably one cycle that caused the subsequent drop in luminosity and a small increase in the intensity of Hα .

Cycles 272-279: The star is getting fainer in all three filters. Minimum was reached in cycle 278 or 279. Close to the minimum metallic shell lines became visible again. The minimum intensity of Hα and Ca II K shell lines was observed in cycle 274, during cycles 274-279 the strength of emission grows.

Since cycle 266: The $U-B$ index was getting gradually redder (even after the minimum luminosity cycle).

Since cycle 279: The UBV luminosity started increasing again.

The authors observe that a similar behavior as the hydrogen emission lines is exhibited by the H I 402.6 line. Let us note that these findings are more accurate than and agree well with the findings of Harmanec et al. [1978].

11. Doazan et al. [1982] also indicated the possibility of very fast short-term variations.

12. In the subsequent paper **?** the authors discussed possible interpretations. Three models are considered: binarity, pulsation and the revolution of an elongated envelope.

    Binarity: Different arguments for the binary hypothesis were already mentioned in the course of this summary, so let us just specify certain details.

    – Phase-locked V/R variations of the Hα shell line could be explained by the periodic revolution of an asymmetric disk. The asymmetry could in turn explained by considering the Be star as a component of a binary system. The asymmetric disk is then created as was described in 1.3.2, note that the model from Harmanec et al. [2002] was in its entirety suggested about twenty years later. The observations corresponds to a disk rotating againts the sense of the binary system. That is V > R when the RV of the Be star is positive.

- The deviations of the Hα RV curve from the RV curve obtained from the mean of the measurements of HI lines are observed in derived phases corresponding to when the stars are in one line with respect to the observer.
- The second absorption core could be attributed to the projection of matter streaming between the two stars.
- The fact that the RV variations are not observed for the Fe I and Ca II K could correspond to a growing external gaseous envelope.
- The question of whether the binary model could account for the long term changes was inspected. By comparing the brightening of the object and the evolution of the intensities of spectral lines relative to the local continuum led the authors to the assumption that the H I and He I lines have their origin in the inspected central star and the shell lines are of a different origin. We see these estimates correspond to the presence of the repeatedly discussed disk or envelope.

  Further a peculiar observation was made: the light curve of the object corresponds to an inverse evolution of a nova. Inverse in the sense that where a decrease would be observed for novae an increase i seen and vice versa. It is noted that as a variation is beginning to be observed for novae an increase in hydrogen emission accompanies it. We may once again take this to be an argument for the presence of a gaseous disk.

Pulsation: An earlier model involving non-radial pulsations than is described in 1.3.3 was also considered to account for the RV variations (Baade [1988])). No calculations were made for 88 Her based on this model due to the lack of knowledge of true rotational velocities of the star and the corresponding pulsation period of a non-rotating object. It is further noted that this model could in principle explain some of the other observed long-term and medium-term variations. In conclusion pulsation could be considered as a viable model and likely plays a role in certain Be systems but with measurements available at that time it could not be proven or disproven for 88 Her.

Revolution of an elongated envelope: The last model discussed by the authors as a possible explanation for the observed RV and V/R changes is based on the model described in 1.3.1 further developed by many authors. The possibility of the revolving of an envelope caused by binarity was already discussed. A mechanism for the creation of such a envelope around a single star was not available, so a discussion was led under the assumption that such a mechanism exists. Arguments have been put forth that due to strict and unchanging periodicity of the RV and V/R variations despite the dramatic long-term changes it seems unlikely that this model would be realized for 88 Her. If an envelope is really present it is sensible to assume that the varying Balmer emission is evidence of its changes and so one would also expect changes in the RV periodicity.

13. Barylak and Doazan [1986] extended the light curve with observations from

1972-1983 and also studied the long-term variations in the far UV part of the spectrum. They showed that luminosity for different wave lengths in the UV spectral region evolved in the studied period in the same basic manner as in the visible region. That is the UV luminosity decreased when luminosity in before studied filters decreased and so on. The describe the time line of the luminosity of the far UV region in the following manner:

1972-1976: In all the studied regions luminosity does not vary dramatically.

1976/1977-1978: We observe a steep decrease in luminosity in the visible region with a minimum in 1978. There are no photometric measurements for the far UV region between 1976-1978 (that is the last published before the gap measurements are in 1975 a the first after are in 1979). It is assumed that the minimum for the UV region lies in this gap in correlation to the other studied regions.

1978-1979: In the visible region after reaching the minimum in 1978 we see a rapid growth in luminosity. It is assumed that similar behavior occurred in the far UV region. The decrease in luminosity between 1976 and 1979 in the UV region quantitatively is for (where the index represents the studied wavelength in Angstroms); $U_{1565} : 0^{\mathrm{m}}.27$, $U_{1956} : 0^{\mathrm{m}}.38$, $U_{2365} : 0^{\mathrm{m}}.57$, $U_{1565} : 0^{\mathrm{m}}.53$. The authors point out that since the minimum luminosity lies most likely in the observational gap these values present only a lower limit of the real decrease.

1979-1983: The magnitude gradually decreases in all studied regions.

The luminosity variations are also compared to the simultaneous spectral changes. The description of these spectral changes in the overlapping times does no vary from the aforementioned publications but some interesting things are specified. Before we list what is purposeful to point from their findings let us define an useful term used by the authors:

Definition 5 (Quasi-normal B Spectrum)**.** *A spectrum that using (the typically used) low dispersion spectra would be classified as a normal B-type, but on high dispersion spectra a weak shell absorption can be observed in the Balmer lines.*

1972-1976: A quasi-normal B-type spectrum is observed.

1976/1977-1978: A transition from the qausi-normal B-type spectrum to the Be shell spectrum.

1978-1983: The Be shell spectrum evolves; Shell absorption cores and hydrogen emission wings increase in intensity. The authors point out an distinct amendment to the earlier studies comparing luminosity changes with spectral ones: *The time of minimum luminosity in all studied spectral regions does not correspond to the time of maximum intensity of the absorption cores and hydrogen emission wings of the shell lines. Minimum luminosity is reached earlier after as the Be shell spectrum appears and as it evolves with shell lines growing in intensity luminosity in the studied spectral regions increases.*

The steepest change decrease in luminosity happened during the transition while the increase during the development of the shell spectrum was slower. The greatest quantitative differences were in the UV region of the spectrum, but all regions follow the same basic times of decrease and increase.
Colour variations in the studied era are also discussed. The evolution of all colour indices combining the studied UV wavelengths and, U, B and V magnitudes. Let us again summarize the basic aspects of their findings.

- During the transition to the Be shell spectrum (1973-1979) all colour indices combining UV magnitudes and standard magnitudes become redder.
- During the transition to the Be shell spectrum (1973-1979) almost all colour indices combining the different studied wavelengths become bluer, for the exception an explanation is suggested.
- Throughout the studied time interval the least changed indices are: $U-B$ and $U_{1565}-U$

4. Of the Long-term Variations in Brightness and Colour of 88 Her: Theory and Methods

The aim of this chapter is to provide a commentary on the methods used in the discussion and analysis of the obtained data. All calculations, data editing and plots was done via short Python 2. codes that were written specifically for each purpose.

4.1 Obtaining Normal Points

For all data normal points were calculated so that smoother correlations could be inspected. Normal points were obtained separately for each observatory. Let us note that the information that each normal point carries differs. For observatories where multiple measurements in compact time intervals were made normal points represent the mean of measurements that were obtained close in time with one another in the y-axis value and are placed on the x-axis (which represents time) at the half way point between the first and last measurement that is encompassed it that mean. The length of the interval that defined what was considered as close measurements with one another was chosen for each observatory so that the obtained trend was visible as well as possible and to best accommodate the method of that specific station.

For some computations a further smoothing was used. Where it proved useful the normal points were exchanged for average points of these normal points. The average points were calculated the same way from normal points as were normal points from individual measurements but for all observatories together. This was done especially for the study of intervals which are dramatically unevenly covered.

4.2 Transformation of Data into the Johnson system

The Johnson Photometric system in which all results in this thesis are given was described in 2.1. Data form the Hipparchos mission and the KELT telescope have been used alongside data from observatories that observe in the *UBVR*filters. Here a description of the used transformation will be provided.

4.2.1 Hipparchos magnitudes

Hipparchos instrumental magnitudes H_p of 88 Her were transformed into Johnson V and B magnitudes as described by Harmanec [1998]. The magnitudes V and B can be obtained if colour indices $B-V$ and $U-B$ are known using non-linear equations 4.1 and 4.2. Values of coefficients α_i and β_j were used as derived by

Harmanec [1998] .

$$V = H_p + \alpha_1(B-V) + \alpha_2(U-B) + \alpha_3(B-V)^2 + \alpha_4(B-V)^3 + \alpha_5 \qquad (4.1)$$

$$B = H_p + \beta_1(B-V) + \beta_2(U-B) + \beta_3(B-V)^2 + \beta_4(B-V)^3 + \beta_5 \qquad (4.2)$$

As the $B-V$ index is used for the transformation the coefficients must be codependent as shown in 4.3.

$$\beta_1 = 1 + \alpha_1,\ \beta_2 = \alpha_2,\ \beta_3 = \alpha_3,\ \beta_4 = \alpha_4,\ \beta_5 = \alpha_5 \qquad (4.3)$$

The computations that implement these equations were done with a Python 2. script. The key problem of the transformation was the modeling of the colour indices for the corresponding time interval. Measurements from Hvar, Mt. Hopkins and Toronto were used; normal points were calculated but not individually for each observatory but for all measurements together. The obtained normal points were fitted with a polynomial curve; for the $B-V$ index a polynomial of the fifth degree was used and for the $U-B$ index a polynomial of the third degree was used. These polynomial functions were then used for described transformations.

4.2.2 KELT measurements

Measurements from the KELT project were used to prolong the curve in the R filter. The transformation of the KELT magnitudes to R was done on the basis of intuition and so it is to be noted that the final representation carries especially a qualitative information about the trend and any quantitative conclusions should be viewed with this in mind.

The KELT magnitudes were obtained with a few cameras. The original data was very scattered but under further inspection it seemed that the trend could be best seen from measurements made by the first camera. A lower and higher limit to what seemed like realistic results was guessed at the beginning and at the end of the measurements. These two points each for the lower and higher limit yielded two linear functions that defined the accepted higher and lower limit of magnitudes along the entire interval of measurements. The cleaning process is represented in figure 4.2.2

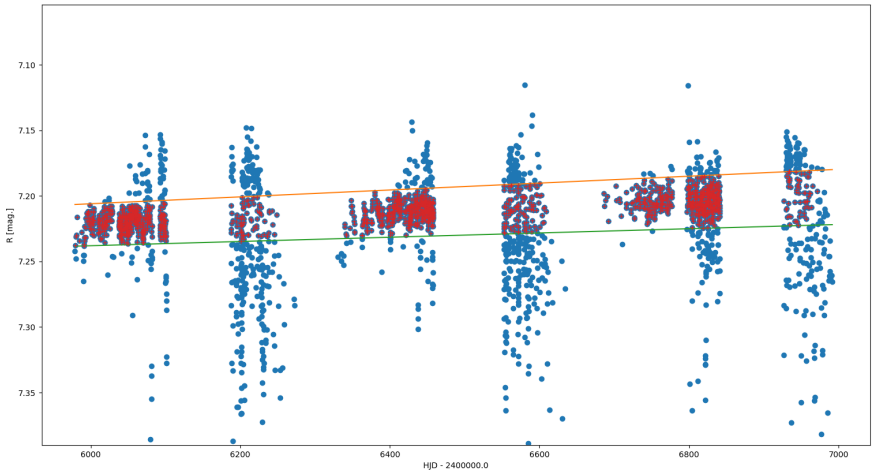

Figure 4.1: The cleaning of the data from KELT

For the so cleaned data normal points were calculated and the data was used in R. No exact transformation exists but the smooth almost linear trend of this interval permitted the data to be aligned next to the observations from Hvar so that in the overlapping interval the magnitudes would correspond.

4.3 Determining the Uncertainty of the Given Values

- For all values of normal points the maximum errors are given.
- For the calculated means of normal points the root mean square deviation is always given.
- For the computed fits the error of the convergence given by Numeric Python are given.

5. Of the Long-term Variations in Brightness and Colour of 88 Her: Results and Analysis

In this chapter firstly the obtained results will be presented and subsequently discussed. The process of gathering the data was described in the last chapter and will not be further inspected here. Tables of used data are presented in the appendices.

5.1 Obtained Results and Discussion: Variations in Luminosity

In this section an assessment of the data collected for each filter will be led and subsequently in 5.1.5 a comparison of the different luminosity curves will be discussed and represented.

5.1.1 *U* filter

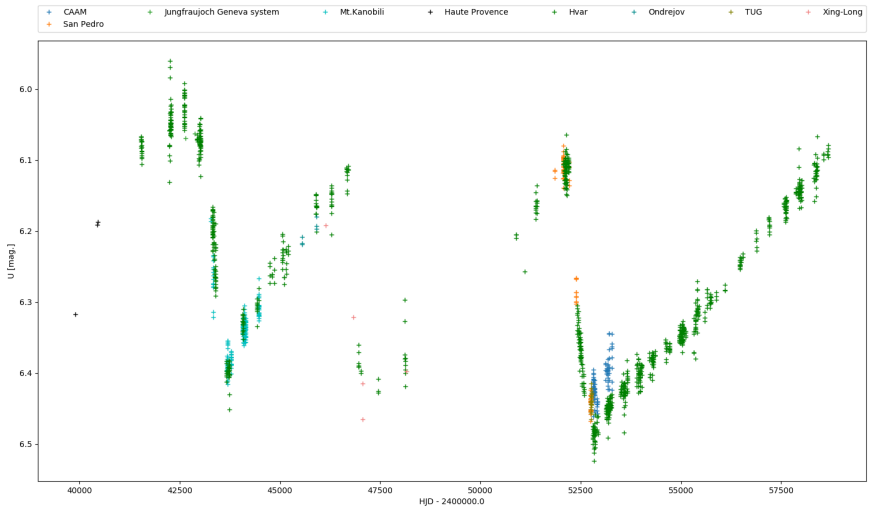

Figure 5.1: Individual obtained measurements in *U*.

The obtained result is highly dependent on the measurements from the Hvar obervatory and the agreement between different observatories is also much worse than in the other filters. Let us especially point out the set of normal points from CAAM during the third cycle that follow a different trend then the measurements from Hvar, for the purposes of further inspection we will use the trend given by the measurements from Hvar as real and omit the CAAM measurements.

The luminosity in the *U* filter evolves in a sort of "zig-zag" fashion, that is

the changes between increases and decreases are sharp and sudden. The increases and decreases seem almost linear. A quantitative overview of the three observed cycles is given in 5.2, let us note on what it contains.

- For each cycle the lowest obtained normal point is noted to represent each minimum.
- For the first cycle the noted maximum of luminosity was calculated as the average of the last three normal points before the drop. For the second cycle the maximum is taken as equal to the last normal point before the drop. For the third cycle the maximum of luminosity was calculated as the average magnitude of normal points between 52000 and 52268.
- The estimated value of the complete drop in luminosity is given as the difference between the given maximum and minimum.

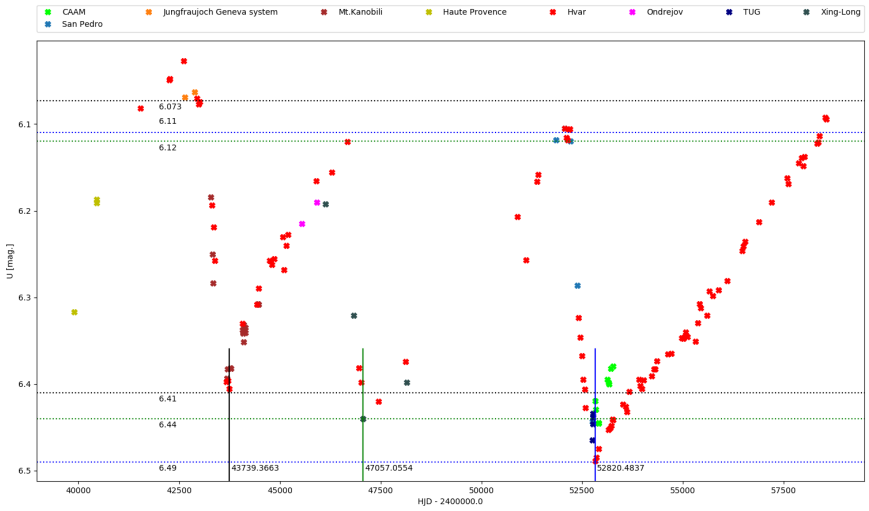

Figure 5.2: Normal points calculated for measurements plotted in 5.1.1. The magnitudes of intervals with maximum luminosity for each cycle are marked and minimal normal points for each cycle.

Considering the aforementioned linearity of the decreases and increases a linear fit of the increases and decrees of the first and third cycle was computed. The coefficients of the best approximation are given in 5.1.

Table 5.1: Coefficients of linear fits in U

	Cycle	
	First	Third
Dec. lin. c.	$7.604 \cdot 10^{-4} \pm 3 \cdot 10^{-7}$	$6.60537 \cdot 10^{-4} \pm 3 \cdot 10^{-9}$
Dec. const. c.	-24 ± 630	-28 ± 8
Inc. lin. c.	$-9.059131 \cdot 10^{-5} \pm 1 \cdot 10^{-11}$	$-6.47402256 \cdot 10^{-5} \pm 6 \cdot 10^{-13}$
Inc. const. c.	10.33 ± 0.02	9.899 ± 0.002

5.1.2 *B* filter

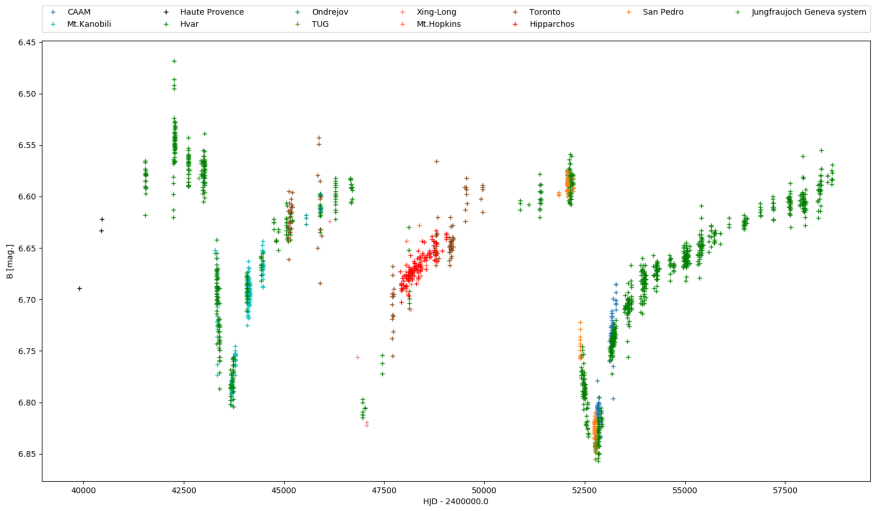

Figure 5.3: Individual obtained measurements in *B*.

The evolution of luminosity in the *B* filter is qualitatively different form the *U* filter. Especially the shape of the increases differs. The increases in this filter have two characteristic parts. The sharp minimum is followed by an interval of steep increase during which about half of the lost luminosity returns. After an abrupt change in the trend a longer interval during which the increases becomes more gradual and the curve smoother follows.

A quantitative overview is given in table 5.2, let us comment on the obtained values.

- For each cycle the normal point with the lowest luminosity is tabled.

- The given maximum luminosity for the first and third cycle is equal to the mean magnitude of normal points during the interval of constant luminosity of that cycle. For the second cycle the given value is equal to the magnitude of the last point before the steep drop in luminosity.

- An estimate of the drop in luminosity is given for each cycle. For the first and third cycle the estimate given as the difference of the constant luminosity mean and the minimal normal point. Due to the lack of an observed constant interval the estimate is given as the difference of the last normal point before the drop and the minimal normal point.

- Each cycle has a characteristic section of a steep increase in luminosity following the sharp minimum. The procent given in table 5.2 are a lower estimates of the how much of the lost luminosity returns during this interval.

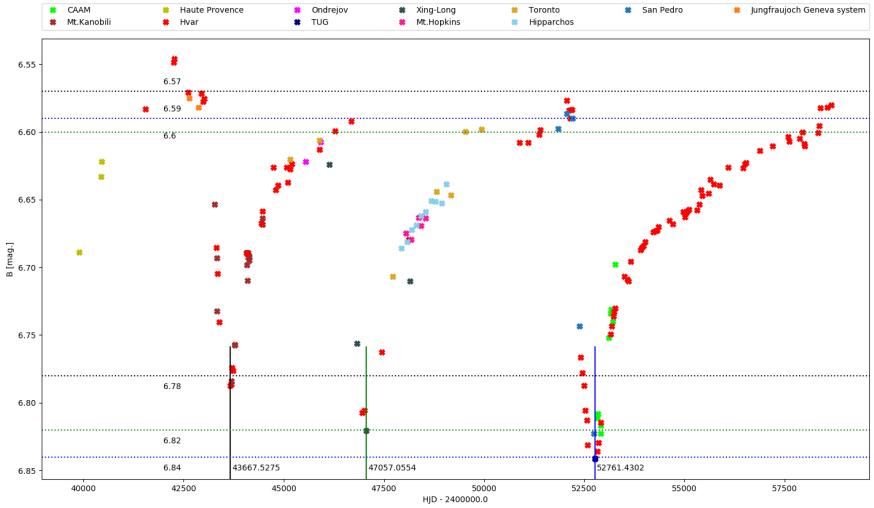

Figure 5.4: Normal points calculated for measurements plotted in 5.1.2. The magnitudes of intervals with maximum luminosity for each cycle are marked and minimal normal points for each cycle.

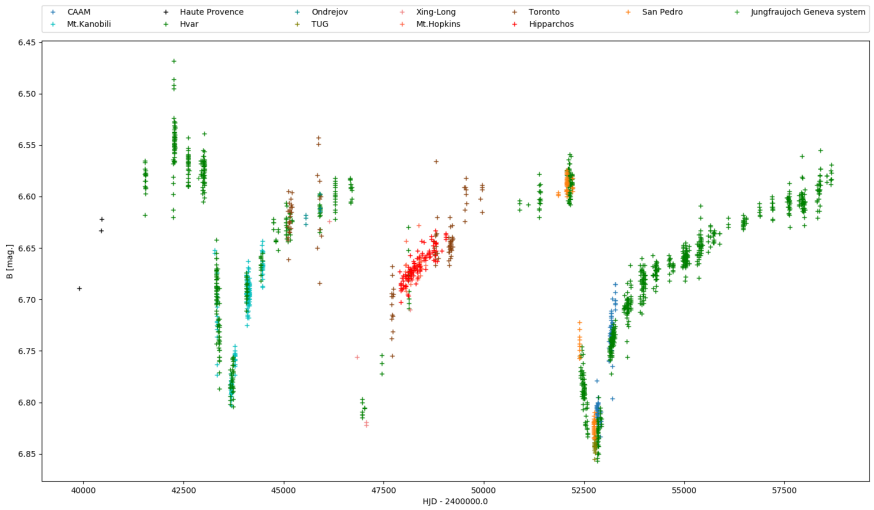

Figure 5.5: Individual obtained measurements in V.

5.1.3 V filter

The evolution of luminosity in the V filter is plotted in 5.1.3 and 5.1.3. A qualitative summary can be found in 5.2. As the curve in V is best covered by measurements and also has the best agreement between observatories a more comprehensive assessment of the obtained data is described.

Most calculated normal points for measurements from different observatories agree together fairly well with the exception of the measurement from Geneva at

42641.4180 which is much lower than the trend of the other measurements. Since this normal point is equal to a single measurement it seems wiser to consider it as false. Another peculiarity are two normal points calculated for measurements from Toronto around 49563 and 49935. Unfortunately they fall within a time interval which is poorly covered but if we consider the trend of the surrounding normal points 5.1.3 we can assume that such a rapid increase probably is not real. On the other hand let us note that the closest normal points on each side seem to also indicate some increase so perhaps some sort of local increase did occur, but here presented data is not sufficient to draw a conclusion.

Let us also point out that the early measurements from Haute Provence are represented by normal point which are equal to singular measurements. They add information about the qualitative trend of luminosity before systematic measurements began but the specific quantities must be considered with a great uncertainty. Let us now describe the three cycles that have been observed:

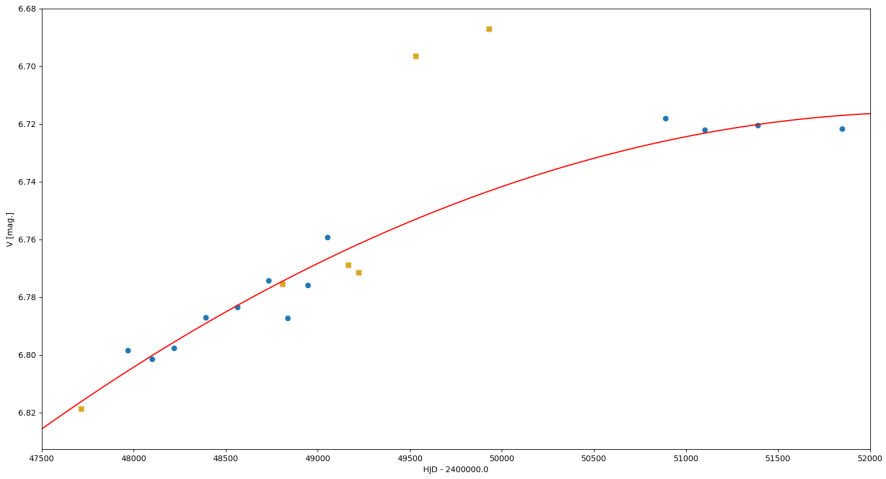

Figure 5.6: A parabolic fit of average points of all normal points (blue) in the vicinity of the measurements from Toronto. We see that the two measurements around 49563 and 49935 are probably false.

First cycle:

1. The aforementioned measurements from Haute Provence indicate the end of a cycle before systematic observations began.
2. Between 41400 and 43050 (1972-end of 1976) the magnitude can within the accuracy of measurements presented here be considered as constant. No fits believable fits could be obtained that would indicate any real trend.
3. Normal points between 43300 and 43450 show and abrupt steep decrease. A good linear fit can be obtained for this part of the curve . A quadratic fit was also computed but the convergence showed the quadratic coefficient very small and so probably made non-trivial only by the uncertainty of the measurements. The abrupt beginning of the decrease is clear. If we accept the binary hypothesis and the period

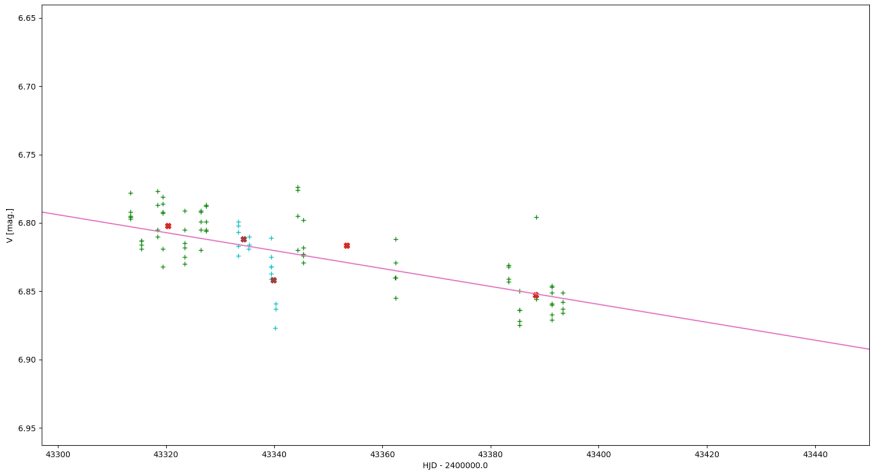

Figure 5.7: A linear fit of the steep decrease at the beginning of the first cycle. The obtained fit corresponds to the equation: $V(\text{HJD} - 2400000) = (6.560 \cdot 10^{-4} \pm 2.54 \cdot 10^{-7})(\text{HJD} - 2400000) + (-21 \pm 477)$. The massive uncertainty in the constant coefficient can be attributed to the fact that the studied points are far from the y-axis. We can assume that in the studied region of the function the outcome will not be affected too much.

of around 87 days we can observe that the length of time between the last measurement before the beginning of the decrease and the first measurement on the decrease is less then three periods. This seems to point to what has already been suggested by Harmanec et al. [1978] that the event causing the decrease is restrained to only a few and perhaps a single cycle. If the linear fit is to be believed we can calculate that the function reaches luminosity of the described constant interval sometime around 43160 ($V(43160) = 6^{\text{m}}.702$). That would leave an interval just over one period. This would point the event causing the decrease to be happen during a single cycle. The unobserved transition into the decrease could in principle be represented by a smoother curve but a comparison with the other two observed long-term variation cycles would support that a sudden change occurs.

4. The lowest obtained normal point is at 43667 with a magnitude of $6^{\text{m}}.892$ with a maximum uncertainty of $0^{\text{m}}.01$. It is difficult to decide whether the true minimum of luminosity was observed. Although there is no physical justification for this; a quadratic and a cubic function was fitted to all normal points and subsequently to average points of normal points on the steep decrease, around the minimum and up to 44150 where the trend seems to some what change. The intention of these fits was to determine how sensitive the position of the minimum was to these few sensible parameters 4 . More logical to the author seemed the cubic polynomial because the evolution after the minmum according to his guess changed into a concave function. From 4 we can

conclude that although the position of the minimum sages relative to the degree of the used polynomial the minimal magnitude falls always within the error of the lowest measured magnitude. Also we observe that the locally the fit is not sensitive to whether normal or average normal points are used, which can be taken as a reassurance of the reached conclusion.

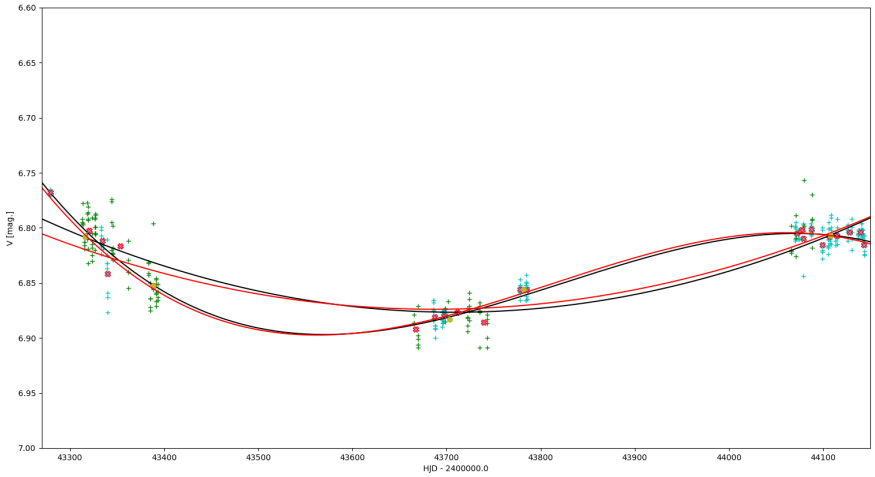

Figure 5.8: An experiment with different fits to determine if the observed lowest luminosity corresponds to the true minimum. Since this fit is of interest only in a qualitative sense the computed coefficients are omitted. Two quadratic and two cubic fits were computed; for each degree on with respect to the normal points and one with respect to the average normal points.

Following the above depicted argumentation we can only set an upper limit to the duration of the minimum luminosity; from the position of the obtained measurements it is clear that the minimum lasted less then a year. If we compare the shape of the minimum with the other two cycles it seems quite viable that the occurring shape of the minima is rather sharp.
An estimate of the whole drop in luminosity was calculated as $6.892 - 6.696 = 0^{\mathrm{m}}.196$ where the minuend is the value of the lowest normal point and the subtrahend is the mean of the normal points in the part of the light curve with constant luminosity. The mean is given in all places in which it is equal to the mean of the average points of the normal points from that section. The estimate can be accepted as a lower limit of the decrease with a maximum error of $0^{\mathrm{m}}.02$.

5. From the sharp minimum till about 44170 (Second half of 1979) a steep increase in luminosity is observed. About 43% of the lost luminosity returns (the highest average of normal point in this section shows a magnitude of $6^{\mathrm{m}}.807$). This quick increase is not as steep as the decrease the linear coefficient of a calculated linear fit of normal points on this part of the curve is $-1.784444 \cdot 10^{-4} \pm 1.1 \cdot 10^{-10}$.

6. The end of the cycle is characterized by a gradually increasing luminosity with a much smoother curve. At firt inspection of 5.1.3 and 5.1.3 a question arises; does the luminosity reach its former maximum or is the star getting fainter with time. From visually comparing the beginning and end of this cycle it could seem that the original luminosity was not reached. On the other hand if we compare the later maxima of luminosity it seems that they no longer decrease. This drop from the first to the second observed maximum is a peculiarity and it is not clear whether it is caused by the uncertainty of the earlier measurements or whether it is real. It is also to be noted that the end of this cycle (beginning of the second one) is not very well covered, to this we can attribute the fact that no real section of constant luminosity is observed.
7. The maximum normal point around this second luminosity maximum is at 46680.3475 with a magnitude of $6^{\mathrm{m}}.71 \pm 0^{\mathrm{m}}.02$.

Second cycle: The second cycle is much more poorly covered because of the war in Yugoslavia. The basic trend is the same for all three cycles. So let us give only a shorter quantitative description.

1. As has already been said the basic qualitative trend remains the same. It begins again with an abrupt decrease in luminosity. Since for this part of the curve not many measurements have been obtained it seems pointless to try and describe it by a linear fit.
2. The minimum normal point obtained for this cycle is at 47057.05535 with a magnitude of $6^{\mathrm{m}}.915 \pm 0^{\mathrm{m}}.01$, from the contour of the curve we can guess that the real minimum is probably very close to this measurement. We can once again make an quantitative estimate of the whole decrease; since no section of constant luminosity can be determined the difference between the minimum normal point and the last normal point before the decrease will be used; $6^{\mathrm{m}}.915 - 6^{\mathrm{m}}.712 = 0^{\mathrm{m}}.203 \pm 0^{\mathrm{m}}.025$.
3. The steep increase following the sharp minimum lasts till at least 47714.134 and at least 48% of the lost luminosity returns.
4. The end of the cycle is again characterized by a smooth gradual increase in luminosity (47800-50100) and the a short period of constant luminosity. For the interval that can be considered as of almost constant luminosity measurements have been obtained between 50765 and 52253. The mean of normal points in this section of the curve is $6^{\mathrm{m}}.712 \pm 0^{\mathrm{m}}.02$. Let us note that this is in very good correspondence with the the preceding luminosity maximum.

Third cycle: The third observed long-term variation cycle is perhaps the best covered by measurements especially by the systematic effort at the Hvar Observatory. Once again in is good to underline that the basic qualitative trend does not change.

1. A linear fit for the abrupt steep decrease at the beginning of this cycle 1. Unfortunately it is not possible to repeat the argumentation showing

that the event causing the decrease is restricted to a single cycle using this obtained fit as well as in the case of the first cycle because the computed function reaches luminosity equal to the constant part of the curve somewhere in the constant interval. It is still possible to take this as an qualitative argument that the time for the event to take place is limited.

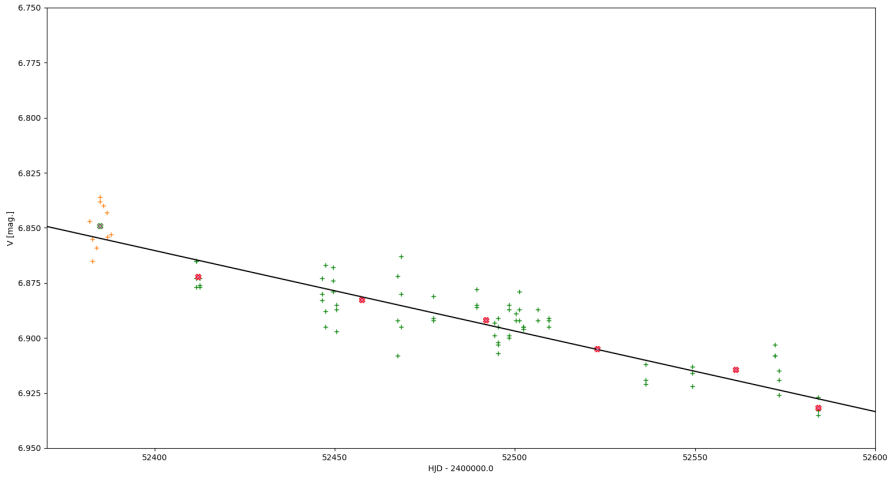

Figure 5.9: A linear fit of the steep decrease at the beginning of the third cycle. The obtained fit corresponds to the equation: $V(\mathrm{HJD} - 2400000) = (3.65491 \cdot 10^{-4} \pm 1.3 \cdot 10^{-9})(\mathrm{HJD} - 2400000) + (-12 \pm 4)$.

2. The minimum was inspected once again via a similar experiment like the minimum of the first cycle. Again it shows (here perhaps more persuasively) that the real minimum is well captured by the normal points of the measurements. Let us again obtain an estimate of the decrease as in the case of the first cycle: $6^{\mathrm{m}}.9366 - 6^{\mathrm{m}}.712 = 0^{\mathrm{m}}.22 \pm 0^{\mathrm{m}}.02$ where the minimal obtained normal point is at 52769.352.

3. For the following steep increase just the same quantities as for the other cycles will be listed. To compare the steepens of the increase with the decreases a linear for normal points between 52724 and 53336 was obtained 4. An estimate of the precentage of the lost luminosity was calculated using this linear fit;

$$\frac{[6.9366 - V(53283)]}{0.22} = 51\%.$$

4. The rest of the obtained curve is again a smooth gradual increase in luminosity. Let us note that this well covered cycle indicates that the change of pace of the curve is quite sudden.

At the end of our discussion of the obtained evolution of luminosity in the visual part of the spectra by a few notes;

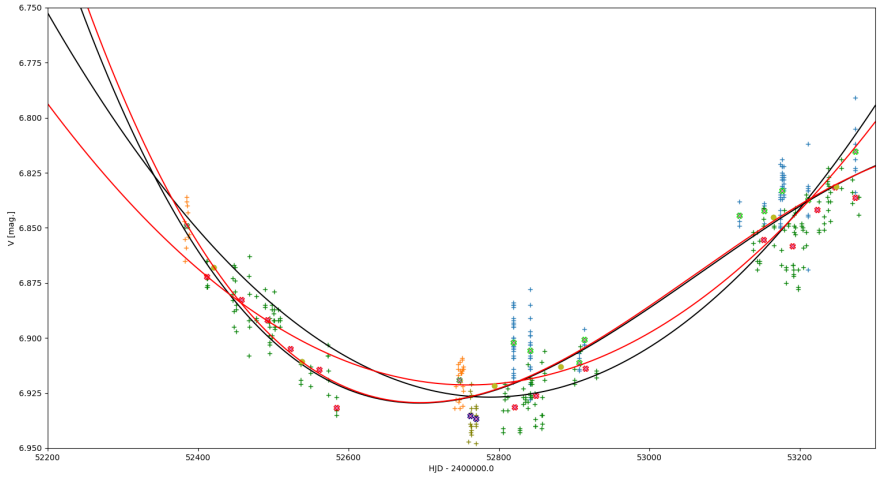

Figure 5.10: An experiment to determine the credibility of the third luminosity minimum.

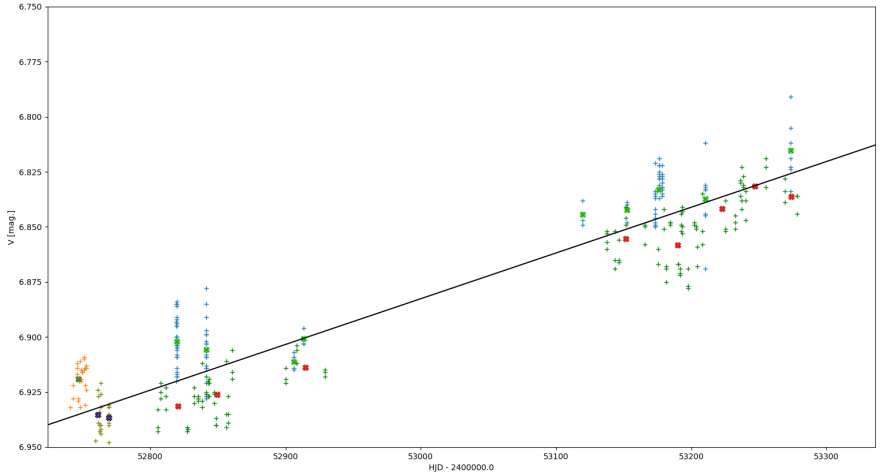

Figure 5.11: A linear fit of the steep increase during the third cycle. The obtained fit corresponds to the equation: $V(\text{HJD} - 2400000) = (-2.07662 \cdot 10^{-4} \pm 1.8 \cdot 10^{-10})(\text{HJD} - 2400000) + (-17.8 \pm 0.5)$.

- As has already been mentioned after the first cycle it seems that the value of maximum luminosity is reached. A different tendency may be indicated by the minima. The identified minimal normal points for each cycle decrease in luminosity with each cycle ($6^{\text{m}}.892$, $6^{\text{m}}.915$, $6^{\text{m}}.9366$).

- The identified normal points of minimal luminosity for each cycle are located at 43667.5257, 47057.0554 and 52765.3520 that is in 1978, 1987 and 2003. We see that that no periodicity is indicated.

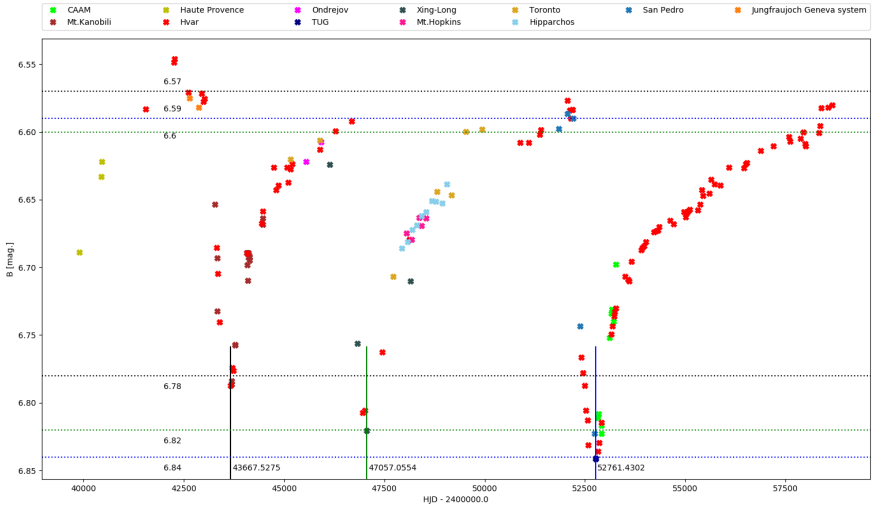

Figure 5.12: Normal points calculated for measurements plotted in 5.1.3. The magnitudes of intervals with maximum luminosity for each cycle are marked and minimal normal points for each cycle.

5.1.4 *R* filter

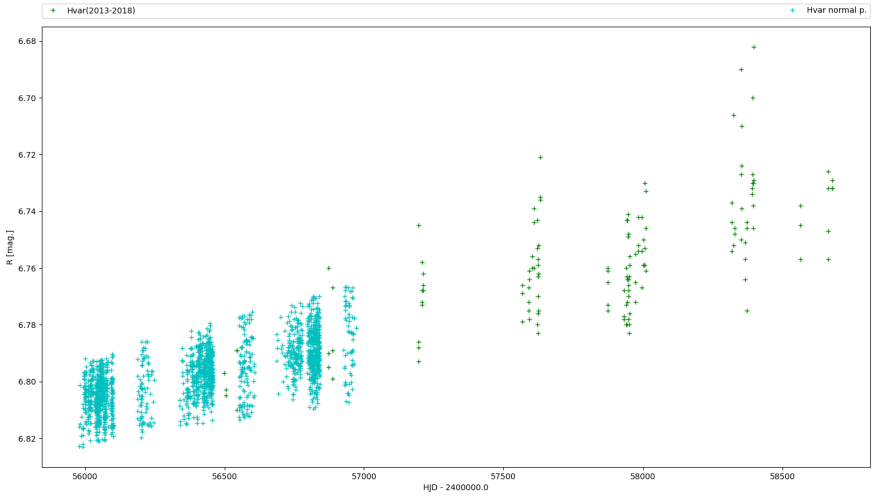

Figure 5.13: Individual obtained measurements in R.

The evolution of luminosity in the R filter is plotted in 5.1.4 and 5.1.4. There is not a whole lot of information that can be extracted from the short interval of observations that has been obtained. It can be said that there is a certain correspondence to the evolution of luminosity in the other filters because the curve is also increasing in this interval. Father from the comparison with the other regions; since it seems that all regions are nearing to the former maximum

luminosity we can make a lower estimate of the maximum luminosity for the R filter. The mean of the last five obtained normal points is $6^{\mathrm{m}}.737 \pm 0^{\mathrm{m}}.006$.

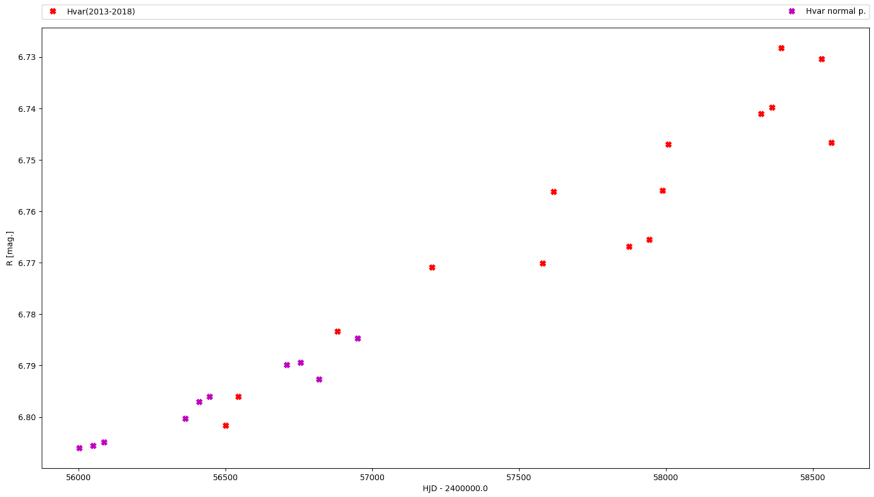

Figure 5.14: Normal points calculated for measurements plotted in 5.1.4.

5.1.5 *UBVR* Summery

Table 5.2: *UBV* Evolution of the Luminosity

		Cycle		
		First	Second	Third
U	Min. [HJD]	43739.3663	47057.0554	52820.4837
	Min. [mag.]	6.41 ± 0.01	6.44 ± 0.025	6.49 ± 0.02
	Max. [mag.]	6.073 ± 0.002	6.120 ± 0.003	6.110 ± 0.006
	Drop [mag.]	0.33 ± 0.012	0.32 ± 0.028	0.38 ± 0.026
B	Min. [HJD]	43667.5275	47057.0554	52761.4302
	Min. [mag.]	6.78 ± 0.02	6.82 ± 0.01	6.84 ± 0.015
	Max. [mag.]	6.57 ± 0.01	6.60 ± 0.02	6.59 ± 0.008
	Drop [mag.]	0.21 ± 0.03	0.22 ± 0.03	0.24 ± 0.023
	Steep [% of lost]	62%	55%	46%
V	Min. [HJD]	43666.6455	47057.0554	52769.352
	Min. [mag.]	6.89 ± 0.01	6.92 ± 0.01	6.94 ± 0.01
	Max. [mag.]	6.70 ± 0.02	6.71 ± 0.02	6.71 ± 0,02
	Drop [mag.]	0.20 ± 0.03	0.203 ± 0.025	0.22 ± 0.02
	Steep [% of lost]	43%	48%	51%

Finally let us summarize the evolution of luminosity in the four studied filters.

- Minimum luminosity is reached within the accuracy of determining the moments of true minima at the same time in U, B and V.

- Qualitatively the V and B magnitudes follow the same contour. The U magnitude differs especially in the shape of the luminosity increases after each magnitude maximum is reached while for B and V regions the increases are characterized first by a steep part and after 40% - 60% of the lost luminosity returns the curve suddenly changes pace and becomes smoother and the increase more gradual, in the U region the whole increase is uniform and almost linear.

- The U region of the spectra also shows the largest drops in luminosity during each cycle. The observed drops in luminosity for the V and B regions have a magnitude of around $0^{\mathrm{m}}.2$ (perhaps slightly higher for B) while in the U region the drops have a magnitude over $0^{\mathrm{m}}.3$.

- The question that has been put forth during the inspection of the different regions of the spectra of whether the star is getting fainter with time as a whole or perhaps whether the observed minima are getting deeper can also inspected while compering B, V and U magnitudes. All three regions seem to show that after the first cycle the remaining maxima seem to always return to the same maximum (even the the most recent observations show a magnitude equal to that of former maxima) while the drops in luminosity seem to increase and the minima get deeper.

5.2 Obtained Results and Discussion: Variations in Colour

In this section the colour changes corresponding to the luminosity variations will be commented through the inspection of colour indices.

5.2.1 $B-V$ Index

The evolution of the $B-V$ index is plotted in 5.2.1 and 5.2.1. In comparison to the obtained curves for luminosity the variations in this index have very small amplitudes and so the figure shows a greater scatter even in normal points and generally is more chaotic. The agreement between different observatories is much worse and it is difficult to decide which points are more believable form these figures so the falsehood of the measurements has to be decided from the luminosity evolution.
We see that each decrease and increase in luminosity is accompanied by a colour variation.

- It is hard to determine much about the contour of the curve from first and second cycle so only the third cycle colour variation will be commented form a qualitative perspective.
  The star varies in colour from its normal state in this index for a shorter interval than in luminosity. The variation takes place during the steep decrease in luminosity and during the steep section of the increase. During the gradual luminosity growth the value of this index is equal to its normal state. The maximum of the colour change corresponds to the minimum of

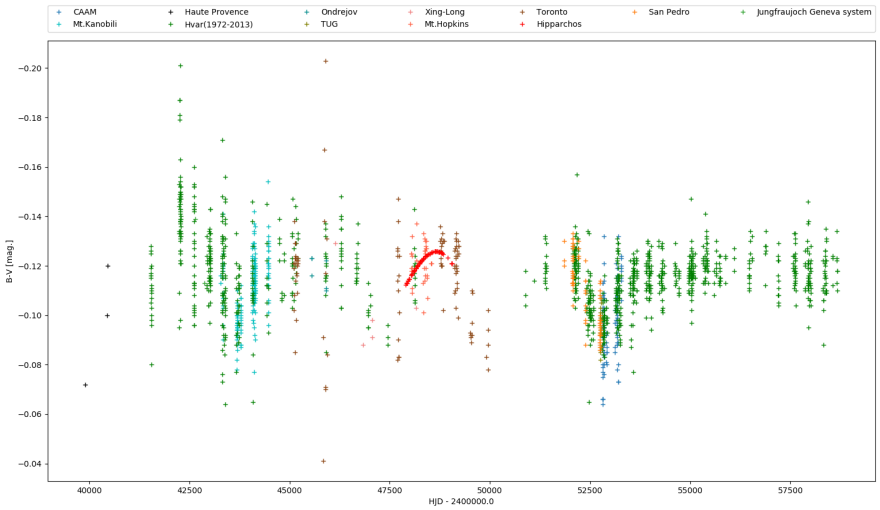

Figure 5.15: Individual obtained measurements of the $B-V$ index .

the luminosity.
The variation is characterized by the index getting redder and then more steeply bluer. To describe the steepens of these changes a linear fit was computed for both sides 5.3 where A represents the linear coefficient and B represents the absolute coefficient.

Table 5.3: Linear fits of the third cycle colour variation

Normal points 52028-52989		Normal points 52985-53355	
A	B	A	B
$3.958069 \cdot 10^{-5} \pm 2 \cdot 10^{-11}$	-2.18 ± 0.05	$-1.21698 \cdot 10^{-4} \pm 6 \cdot 10^{-9}$	6 ± 17

- The mean of normal points outside the colour change intervals is

$$(B-V)_{mean} = -0^{\mathrm{m}}.1201 \pm 0^{\mathrm{m}}.0036 \ .$$

- For each cycle the extreme point is noted in 5.4. We see that each drop in luminosity is accompanied by reddening of around $0^{\mathrm{m}}.03$ in the $B-V$ colour index.

Table 5.4: Extreme normal points

[HJD – 2400000]	43693.8083	46833.3557	52913.2795
[mag.]	-0.095 ± 0.01	-0.088 ± 0.01	-0.084 ± 0.005

- A peculiarity is indicated in evolution around 50000. The normal points in this interval seem to show another variation that does no correspond to the luminosity changes. Unfortunately it falls within section that is only poorly covered by obtained measurements. Let us note that the most peculiar points are the two points from Toronto that have been already identified as problematic but surrounding points from other observatories also show a tendency of change towards the red. A similar discussion was led referring to the luminosity in the V filter. It does not seem wise based on this data to draw a conclusion on whether this peculiarity points to a real event or to make quantitative estimates but it could be that some brightening in the V region occurred.

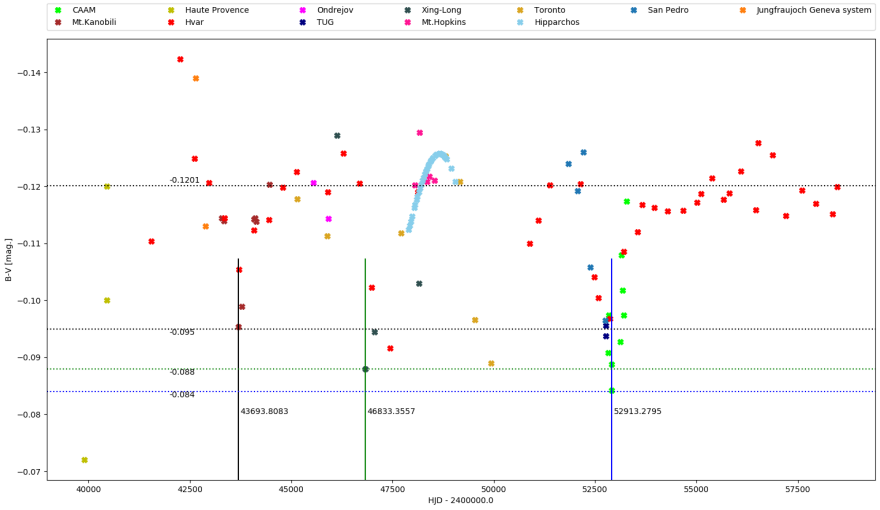

Figure 5.16: Normal points calculated for measurements plotted in 5.2.1. The mean of normal points outside the variation intervals and extreme normal points for each cycle are shown.

5.2.2 $U-B$ Index

The evolution of the $U-B$ index is plotted in figures **??** and **??**. The agreement between the different observatories is very good and the obtained contour has a low scatter.

On first sight it is noteworthy that the $U-B$ index is on this long-term scale practically always changing, basically no intervals of a constant value of the index have been observed. For this evolution a quantitative and qualitative description can be led for the whole observed period.

- The extreme points of each cycle (maxima in magnitude) do not correspond to the observed luminosity minima but rather occur about a year and halve later.

- Each cycle is characterized by a smooth curve with an initial reddening and subsequent return to the initial value. All three cycles can be well modeled

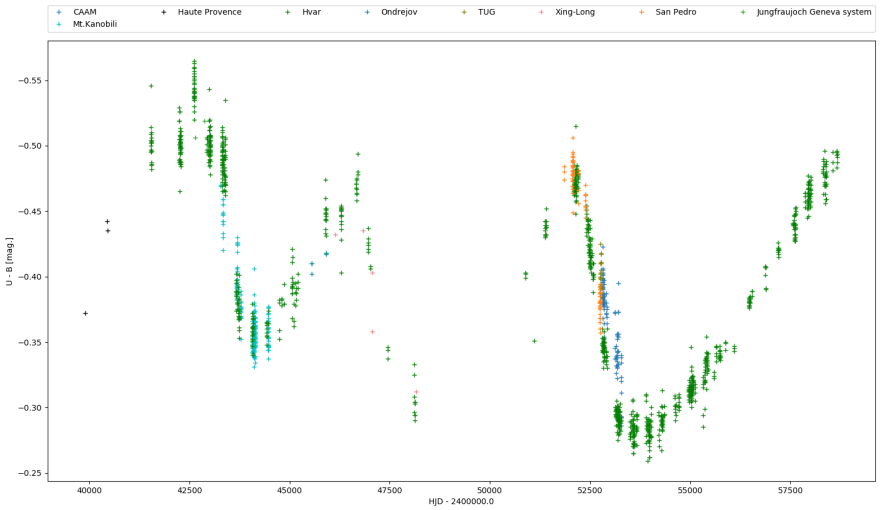

Figure 5.17: Individual obtained measurements of the $U-B$ index .

by polynomial functions; for the fist and second cycle the best fit seemed a cubic polynomial, the third cycle could be modeled well even by a fourth degree polynomial 5.2.2.

- For each cycle the bluest values of the index were calculated and are noted in 5.5. For the first cycle the mean of normal points between 41327 and 43141 is given, for the second cycle the value of the last point before the reddening is given and for the third cycle the mean of points between 52000 and 52300 is given.

Table 5.5: The bluest points for each cycle

Cycle		
First	Second	Third
-$0^{m}.510$ ±$0^{m}.012$	-$0^{m}.47$ ± $0^{m}.02$	-$0^{m}.473$ ± $0^{m}.004$

- The most red points of each cycle were calculated as the extremes of functions that were computed as the fits plotted in 5.2.2.

Table 5.6: Extremes of functions that were determined as the fits of the obtained normal points

Cycle		
First	Second	Third
-$0^{m}.355168$	-$0^{m}.28221$	-$0^{m}.284888$

We observe that during the decrease in luminosity the $U-B$ colour index shifts towards the red as shown in 5.7 .

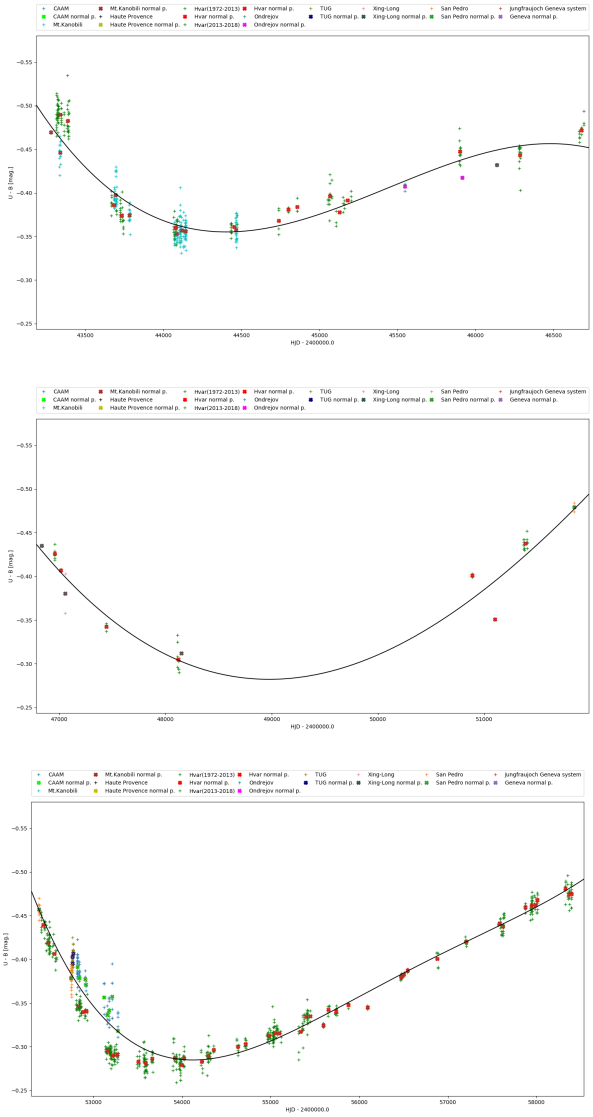

Figure 5.18: The modeling of the three cycles of colour variations. The first figure corresponds to the first cycle the second to the second and the third to the third. For the first and second cycle a third degree polynomial function was used while for the fourth which is best covered by measurements a fourth degree polynomial was used.

- The peculiarity that was discussed in the inspection of the $B-V$ index is not present in the evolution of this index. That is if some abnormal variation in colour did take place where it is indicated then it was probably caused by an event in the V region of the spectrum.

5.2.3 $V-R$ Index

The short interval of obtained measurements of the $V-R$ index is plotted in **??**. Due to the fact that only fairly recent measurements of the R region of the spectrum have been obtained we can not say much about the evolution of this

Table 5.7: The shift towards the red in the $U-B$ index

Cycle		
First	Second	Third
$0^{\mathrm{m}}.155 \pm 0^{\mathrm{m}}.012$	$0^{\mathrm{m}}.188 \pm 0^{\mathrm{m}}.02$	$0^{\mathrm{m}}.188 \pm 0^{\mathrm{m}}.004$

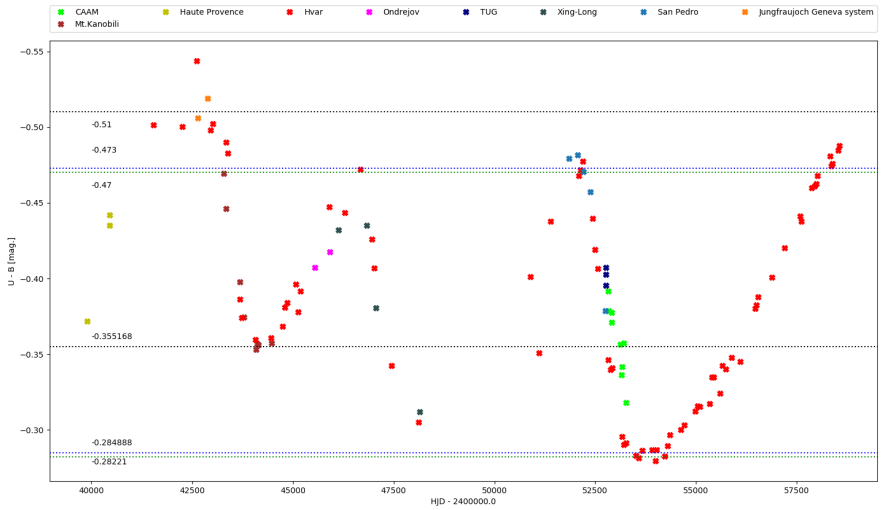

Figure 5.19: Normal points calculated for measurements plotted in 5.2.2. The mean of normal points outside the variation intervals and extreme normal points for each cycle are shown.

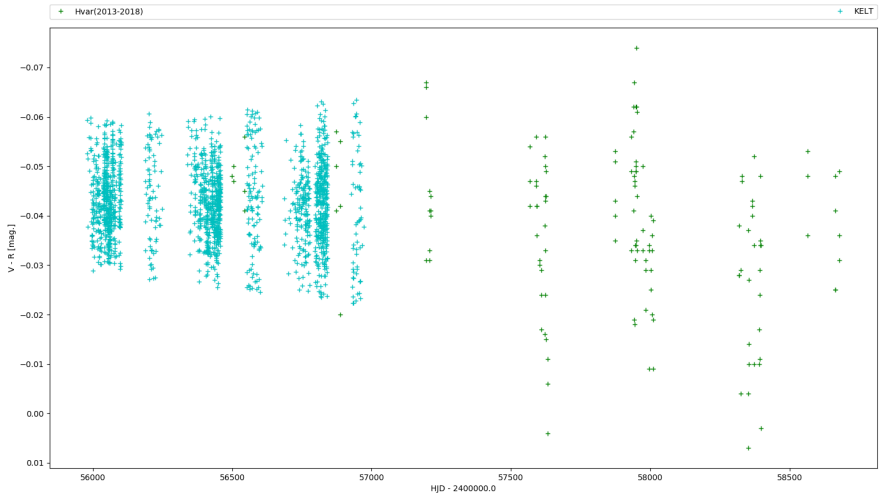

Figure 5.20: Individual obtained measurements of the $V-R$ index.

index. Let us note that during the gradual increase in luminosity observed in R and V a slight decrease in this index is indicated that is it is getting bluer.

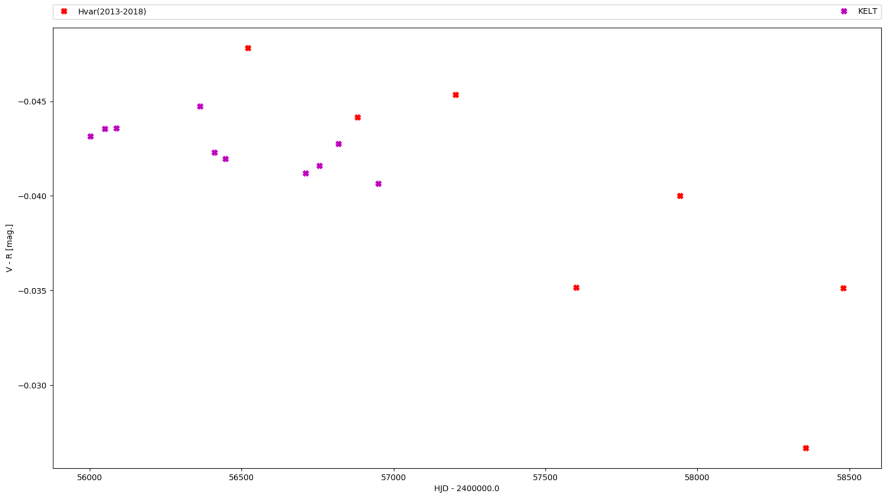

Figure 5.21: Calculated normal points for data plotted in 5.2.3.

5.3 Obtained Results and Discussion: Comparison of the Photometric Variations with the Evolution of Hα Emission

The evolution of the Hα emission line as used for the comparison with luminosity variations i plotted in 5.3 and 5.3. The given relative intensities are calculated as the average intensity of the V and R peak of the emission line with respect to the spectral continuum. In the following discussion we will assume that star is being observed roughly edge-on and we shall show that under this assumption the obtained results correspond to what has been decried in chapter one. In the first chapter the term Negative correlation was defined and 88 Her was given as an example of an object exhibiting this kind of correlation. Let us compare the basic characterization of a Negative correlation with the result presented in 5.3 and 5.3. The expected behavior described by the definition of the Negative Correlation would mean that the strength of the Hα emission line directly corresponds in time to the loss of luminosity. A comparison of the first observed photometric variation cycle with the evolution of the Hα line shows that this is not the case. In 5.3 the first obtained normal point with an intensity above the continuum is marked. We see that the emission started to be observed about 200^{d}before the minimum of luminosity and then steeply gathered strength and reached its local the maximum during the phase of gradual increase in V and B. In the third cycle we can compare the local maximum of emission intensity with the variations in luminosity. The same behavior is shown; the maximum is reached during the phase of gradual increase in V and B. This amendment to the classical view of Be stars was already mentioned in chapter three as one of the important findings of Barylak and Doazan [1986]. Shell emission lines develop during the variation cycle. Let us note that the data shows that apart from this amendment the description of the Negative correlation holds well for 88 Her.

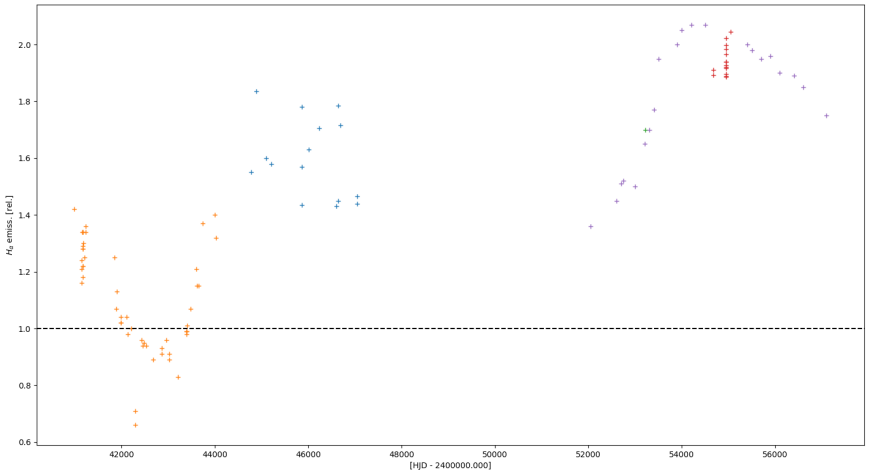

Figure 5.22: Individual obtained measurements of the strength of the Hα emission. Orange points are taken from Doazan et al. [1982], blues points are taken from Duemmler et al. [1988], the single green point is taken from Saad et al. [2006], the orange points are take from Jonák [2016] and the red points are taken from Bhat et al. [2016] .

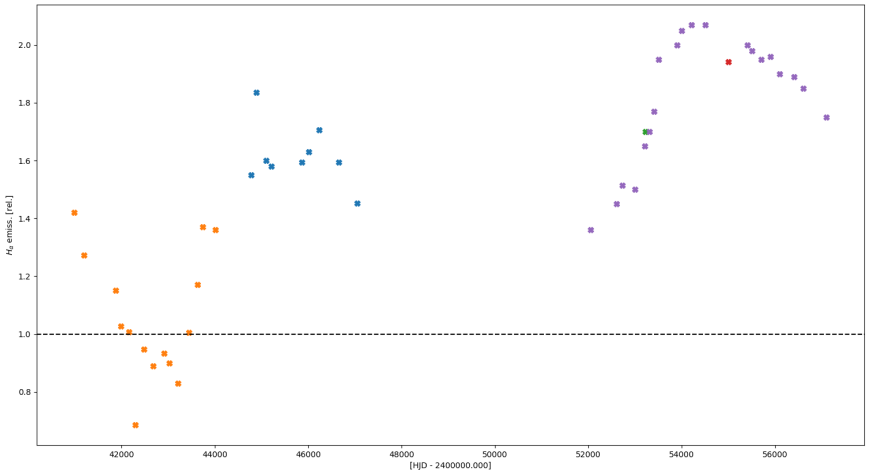

Figure 5.23: Calculated normal points for data plotted in 5.3.

From comparing the maximum in emission from the first and third cycle we can formulate a different correlation between the luminosity variations and the strength of Hα emission; the maximum emission strength of each cycle has a positive correlation to the magnitude of the drop in luminosity of that cycle. Emission during the third cycle reach intensities twice the level of the spectral continuum whilst during the first cycle the emission line reached a relative intensity of only about 1.6. From the previous analysis of the luminosity variations we see that

the with each cycle the depth of the corresponding luminosity minimum increases as does the drop in luminosity.
Another prameter that seems to correlate to the maximum emission strength of the corresponding cycle is cycle length. Using the same comparison as above we can again suspect a positive correlation between cycle length and maximum strength of Hα emission of the corresponding cycle.
If we also take into account variations in colour form 5.4 we can observe that the reddening of the $B-V$ index between the first and third decreases. To conclude the description of the suggested correlation let us summarize:

- There is a positive correlation between the maximum emission strength of a given cycle, the magnitude of the drop in luminosity of the corresponding variation cycle and the length of the cycle.

- There is an inverse correlation to the reddening during each variation cycle.

Now we will assume that this correlation is correct and so assume that the maximum emission of Hα during the second cycle was greater then during than during the first and weaker than during the third. We see that not only is this correlation holds for each cycle but a possible variation on an even longer timescale may be present. During the three cycles A gradual increase in the positively correlated values and a gradual decrease in the amplitude of the $B-V$ colour variations has occurred. Let us underline that the describe changes in luminosity and colour on this even longer timescale are changes of the amplitude of each variation but the values that are reached outside the shell phases seem to remain the same after the first cycle.
Under the aforementioned assumption that the inclination of the axis of rotation is close to $i \approx 90°$a natural explanation of the decrease in luminosity remains an increase in disk size as was described in chapter one. That would mean that the strength of the Calmer shell lines is not directly correlated to the disk size and a more sophisticated model is needed. Let us note that following the described correlation we can once again make a comparison to novae as was noted in chapter three (Barylak and Doazan [1986]). The cycle length of a novae is positively correlated to the strength of the corresponding outburst.

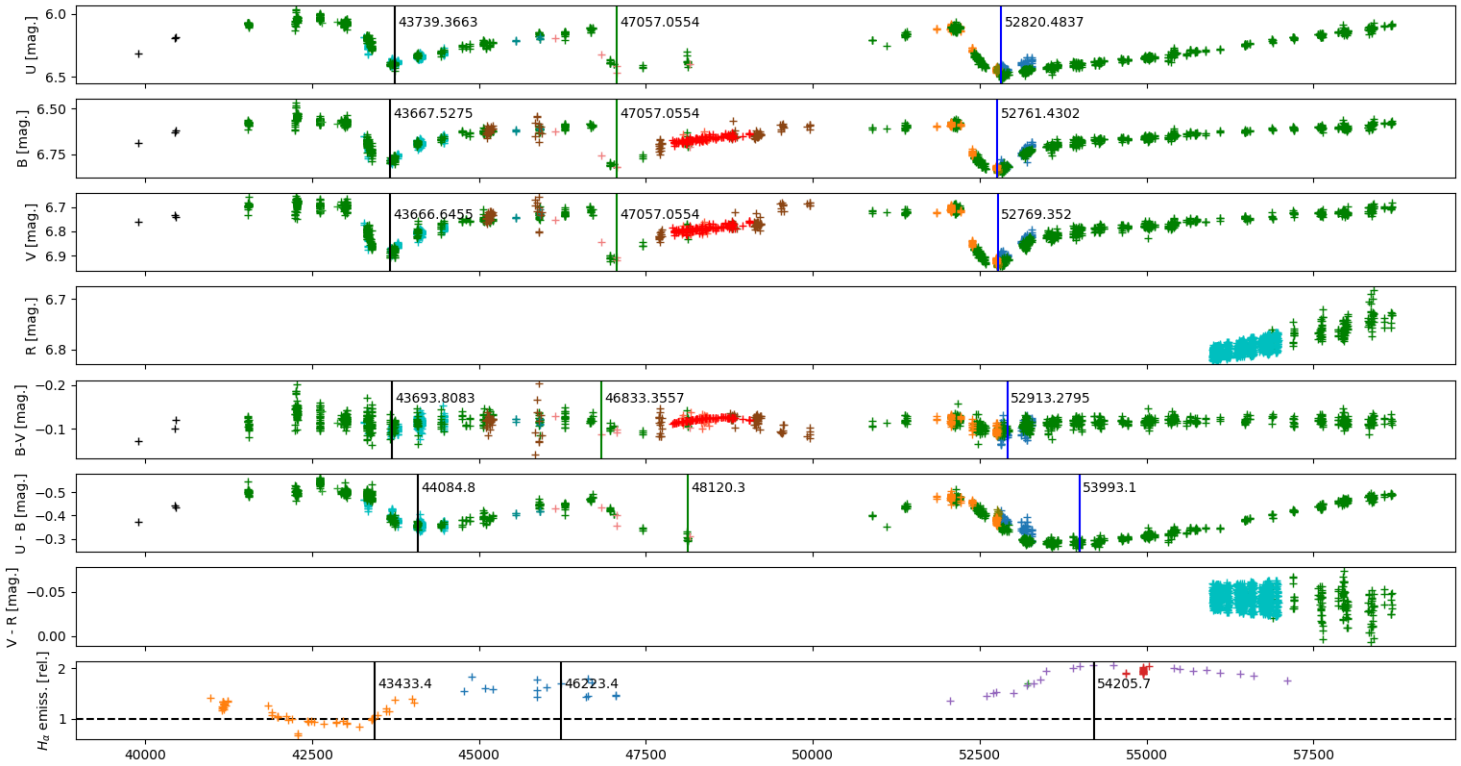

Figure 5.24: A comparison of the variations in light, colour and Hα emission. For all luminosity and colour variations (except R and $V-R$) the extreme normal points for each cycle are marked. For the $U-B$ index the minimal normal points were used. For the Hα variations the first normal point above the continuum during the first cycle is marked and the the identified maxima of the first and third cycle are marked.

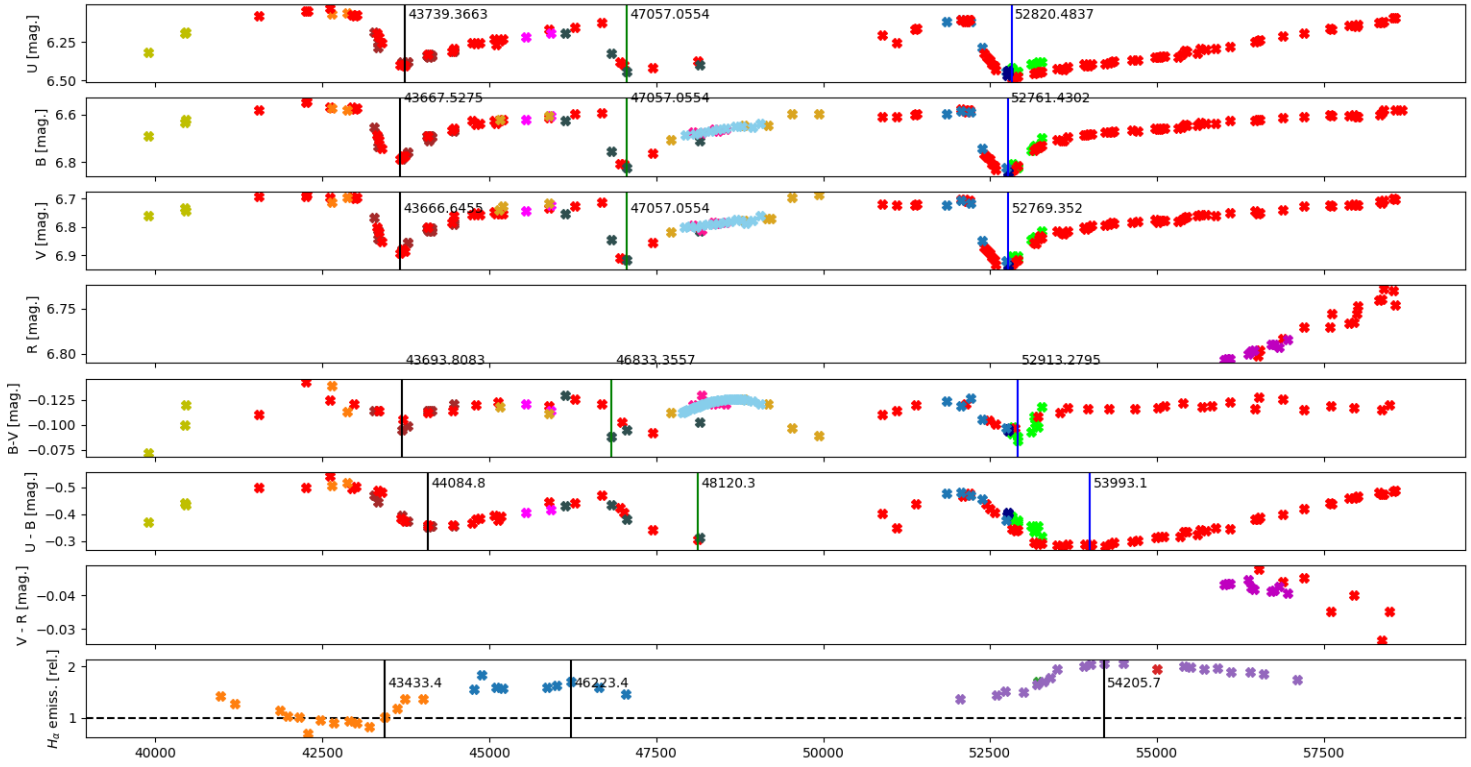

Figure 5.25: The comparison given in 5.3 in normal points.

Conclusion

The analysis of the three observed long-term variations of 88 Her agrees well with earlier publications. Let us list the most important conclusions of this thesis.

- The Shell spectrum develops during the variation cycle and reaches its maximum in the phase of gradual luminosity increase in B and V regions of the spectrum. Apart from this amendment the description of the defined Negative correlation holds well for the system.
- The three cycles show a positive correlation between the depth of the minimum in luminosity, cycle length and maximum strength of hydrogen emission during the corresponding cycle. These values have an inverse correlation to the reddening of of the $B-V$ colour index.
- Altogether the three cycles indicate a gradual change on an even longer timescale.

Assuming the correlation discussed in this thesis is correct the beginning of a new cycle is to be expected very soon.

Bibliography

D. A. Allen. Near infra-red magnitudes of 248 early-type emission-line stars and related objects. **??***jnlMNRAS*, 161:145–166, Jan 1973. doi: 10.1093/mnras/161.2.145.

D. Baade. Nonradial Pulsations and the be Phenomenon. In G. Cayrel de Strobel and Monique Spite, editors, *The Impact of Very High S/N Spectroscopy on Stellar Physics*, volume 132 of *IAU Symposium*, page 217, Jan 1988.

M. Barylak and V. Doazan. Luminosity and colour variations of 88 HER through phase changes fromthe far UV to the visual region. I. A confrontation with traditional Be-star modelling. **??***jnlA&A*, 159:65–74, Apr 1986.

A. Bemporad. La Teoria della Estinzione Atmosferica nella Ipotesi di un Decrescimento Uniforme della Temperatura dell'Aria coll'Altezza. *Memorie della Societa Degli Spettroscopisti Italiani*, 33:31–37, Jan 1904.

Shruthi S Bhat, K T Paul, Annapurni Subramaniam, and Blesson Mathew. Spectroscopic study of be-shell stars: 4 her and 88 her. *Research in Astronomy and Astrophysics*, 16(5):007, apr 2016. doi: 10.1088/1674-4527/16/5/076. URL `https://doi.org/10.1088%2F1674-4527%2F16%2F5%2F076`.

Wiliam P. Bidelman and Sotirios N. Svolopoulos. 88 Herculis: A Bright New Shell Star. **??***jnlPASP*, 72(425):129, Apr 1960. doi: 10.1086/127496.

G. W. Collins, II. The use of terms and definitions in the study of Be stars. In A. Slettebak and T. P. Snow, editors, *IAU Colloq. 92: Physics of Be Stars*, pages 3–19, 1987.

V. Doazan. Long-time variations of the shell star 88 Herculis. **??***jnlA&A*, 27:395, Sep 1973.

V. Doazan, P. Harmanec, P. Koubsky, J. Krpata, and F. Zdarsky. Properties and nature of Be and shell stars 7A. 88 HER Observational data their reduction and basic evaluation. **??***jnlA&AS*, 50:481–490, Dec 1982.

R. Duemmler, A. Kubicela, V. Doazan, B. Bourdonneau, and J. Arsenijevic. The development and weakening of the shell spectrum of 88 Herculis (1977-1987). I. A radial velocity study. **??***jnlA&AS*, 75:311–316, Oct 1988.

M. Dumont, A. Manda, J. Remis, J. Vandenbroere, M. Grenon, B. Kulesza, M. Mikolajewski, K. Ruminski, M. Golebiewski, B. Wikierski, Z. Y. Zheng, X. Zhou, H. Wu, and P. Prugniel. Supernova 1993J in NGC 3031. **??***jnlIAU Circ.*, 5774:2, Apr 1993.

Horn J. Harmanec, P. HEC22 / SORTARCH / VYPAR USER'S MANUAL. January 2017.

P. Harmanec. Review of observational facts about Be stars. *Hvar Observatory Bulletin*, 7(1):55–88, Jan 1983.

P. Harmanec. A reliable transformation of HIPPARCOS H_p magnitudes into Johnson V and B magnitudes. **??***jnlA&A*, 335:173–178, Jul 1998.

P. Harmanec and H. Božić. Forty Years of BV Photometry at Hvar. *Central European Astrophysical Bulletin*, 37:3–8, Jan 2013.

P. Harmanec, P. Koubský, and J. Krpata. Is the shell star 88 HER a binary? *Bulletin of the Astronomical Institutes of Czechoslovakia*, 23:218, Jan 1972.

P. Harmanec, P. Koubský, and J. Krpata. Properties and nature of shell stars. 4. 88 Herculis: the 87-day period confirmed. **??***jnlA&A*, 33:117–121, Jun 1974.

P. Harmanec, J. Horn, P. Koubsky, S. Kriz, F. Zdarsky, J. Papousek, V. Doazan, B. Bourdonneau, L. Baldinelli, and S. Ghedini. Properties and Nature of Be and Shell Stars. 8. Light and Colour Variations of 88 Herculis. *Bulletin of the Astronomical Institutes of Czechoslovakia*, 29:278, Jan 1978.

P. Harmanec, D. V. Bisikalo, A. A. Boyarchuk, and O. A. Kuznetsov. On the role of duplicity in the Be phenomenon. I. General considerations and the first attempt at a 3-D gas-dynamical modelling of gas outflow from hot and rapidly rotating OB stars in binaries. **??***jnlA&A*, 396:937–948, Dec 2002. doi: 10.1051/0004-6361:20021534.

Harmanec, Brož. *Stavba a vývoj hvězd*. Matfyz Press, 2011.

Harmanec,P. *Skripta AST007:ZÁKLADY ASTRONOMIE A ASTROFYZIKY II*. Astronomický ústav Univerzity Karlovy, 2019.

Harmanec,P, Mayer,P, Zache P. *Skripta Dvojhvězdy (AST019)*. Astronomický ústav Univerzity Karlovy, 2019.

R. Herman and M. Duval. Quelques nouvelles étoiles B à émission. *Annales d'Astrophysique*, 25:9, Feb 1962.

H. L. Johnson and W. W. Morgan. Fundamental stellar photometry for standards of spectral type on the Revised System of the Yerkes Spectral Atlas. **??***jnlApJ*, 117:313, May 1953. doi: 10.1086/145697.

Juraj Jonák. A contribution to the study of time variations of the Be star V744 Herculis. *Student Project*, 2016.

Zdenek Kopal. *Close binary systems*. 1959.

S. Kříž and P. Harmanec. A Hypothesis of the Binary Origin of Be Stars. *Bulletin of the Astronomical Institutes of Czechoslovakia*, 26:65, Jan 1975.

Jonathan Labadie-Bartz, S. Drew Chojnowski, David G. Whelan, Joshua Pepper, M. Virginia McSwain, Marcelo Borges Fernandes, John P. Wisniewski, Guy S. Stringfellow, Alex C. Carciofi, Robert J. Siverd, Amy L. Glazier, Sophie G. Anderson, Anthoni J. Caravello, Keivan G. Stassun, Michael B. Lund, Daniel J. Stevens, Joseph E. Rodriguez, David J. James, and Rudolf B. Kuhn. Outbursts and disk variability in be stars. *The Astronomical Journal*, 155(2):53, jan 2018. doi: 10.3847/1538-3881/aa9c7e. URL `https://doi.org/10.3847%2F1538-3881%2Faa9c7e`.

L. B. Lucy and M. A. Sweeney. Spectroscopic binaries with circular orbits. **??***jnlAJ*, 76:544–556, Aug 1971. doi: 10.1086/111159.

F. Mignard. The HIPPARCOS Catalogue : Realization , Content and Scientific Applications. In *AAS/Division of Dynamical Astronomy Meeting*, page 02.01, Sep 1998.

Atsuo T. Okazaki. Long-Term V/R Variations of Be Stars Due to Global One-Armed Oscillations of Equatorial Disks. **??***jnlPASJ*, 43:75–94, Feb 1991.

K. Pavlovski, P. Harmanec, H. Bozic, P. Koubsky, P. Hadrava, S. Kriiz, Z. Ruzic, and S. Stefl. UBV photometry of Be stars at Hvar: 1972–1990. **??***jnlA&AS*, 125:75–98, Oct 1997. doi: 10.1051/aas:1997213.

J. R. Percy, J. Harlow, K. A. W. Hayhoe, I. I. Ivans, M. Lister, R. Plume, T. Rosebery, S. Thompson, and D. Yeung. Photometric Monitoring of Bright Be Stars. III. 1988-89 and 1992-95. **??***jnlPASP*, 109:1215–1220, Nov 1997. doi: 10.1086/133998.

John R. Percy and Akos G. Bakos. Photometric Monitoring of Bright Be Stars. IV. 1996-1999. **??***jnlPASP*, 113(784):748–753, Jun 2001. doi: 10.1086/320806.

Miroslav Plavec. Evolutionary Aspects of Circumstellar Matter in Binary Systems. In Otto Struve and Alan Henry Batten, editors, *Extended Atmospheres and Circumstellar Matter in Spectroscopic Binary Systems*, volume 51 of *IAU Symposium*, page 216, Jan 1973.

Thomas Rivinius, Alex C. Carciofi, and Christophe Martayan. Classical Be stars. Rapidly rotating B stars with viscous Keplerian decretion disks. **??***jnlA&A Rev.*, 21:69, Oct 2013. doi: 10.1007/s00159-013-0069-0.

S. M. Saad, J. Kubát, D. Korčáková, P. Koubský, P. Škoda, M. Šlechta, A. Kawka, A. Budovičová, V. Votruba, L. Šarounová, and M. I. Nouh. Observations of Hα, iron, and oxygen lines in B, Be, and shell stars. **??***jnlA&A*, 450(1):427–430, Apr 2006. doi: 10.1051/0004-6361:20041877.

P.L. Skelton and D.P. Smits. Modelling of W UMa-type variable stars. *South African Journal of Science*, 105:120 – 126, 04 2009. ISSN 0038-2353. URL `http://www.scielo.org.za/scielo.php?script=sci_arttext&pid=S0038-23532009000200013&nrm=iso`.

Otto Struve. On the Origin of Bright Lines in Spectra of Stars of Class B. **??***jnlApJ*, 73:94, Mar 1931. doi: 10.1086/143298.

S. N. Svolopoulos. Spectrum Variability of the Shell Star 88 HER. *Bulletin of the Astronomical Institutes of Czechoslovakia*, 24:167, Jan 1973.

List of Tables

A. Attachments

A.1 References of Used Data

In the tables A.1 and A.2 an overview of observatories and original publications corresponding to the used data,

Table A.1: Data

Name in plots	Observatory	Instrument
Hvar	Hvar,Croatia	0.65-m, DC
Ondřejov	Ondřejov, Bohemia	0.65-m, DC
Xinglong	Xing-Long, China	0.60-m, EMI 6256B
Mt.Hopkins	Mt.Hopkins, Arizona	APT-10 0.254-m
Toronto	Toronto, Canada	0.40-m, EMI 6094
Haute Provence	Haute Provence	0.60-m Lallemand tube UBV
San Pedro	San Pedro Mártir	0.84 & 1.5-m, 13-C 2850m
Geneva	Jungfraujoch Geneva system	-
Hipparcos	–	
TUG	Turkey	0.40-m Cassegrain, SSP5A long
CAAM	Canakkale	0.4-m reflector, SSP-5 photometer
KELT	Apache Point Observatory	The Kilodegree Extremely Little T.

Table A.2: Data

Name in plots	Publications
Hvar	Pavlovski et al. [1997]
Ondřejov	-
Xinglong	-
Mt.Hopkins	Percy and Bakos [2001]
Toronto	Percy et al. [1997]
Haute Provence	Harmanec et al. [1978]
San Pedro	-
Geneva	Dumont et al. [1993]
Hipparcos	Mignard [1998]
TUG	-
CAAM	-
KELT	Labadie-Bartz et al. [2018]